HHS Public Access

Author manuscript

Nature. Author manuscript; available in PMC 2023 February 09.

Published in final edited form as:

Nature. 2022 March ; 603(7902): 728–735. doi:10.1038/s41586-022-04494-7.

A genome-scale screen for synthetic drivers of T-cell proliferation

Mateusz Legut[1,2,3,4,*], **Zoran Gajic**[1,2,3,4], **Maria Guarino**[1,2,3,4], **Zharko Daniloski**[1,2,3,4,‡], **Jahan A. Rahman**[1,2,3,4], **Xinhe Xue**[1,2,3,4], **Congyi Lu**[1,2,3,4], **Lu Lu**[1,2,3,4], **Eleni P. Mimitou**[5,†], **Stephanie Hao**[5], **Teresa Davoli**[4,6], **Catherine Diefenbach**[4], **Peter Smibert**[5,†], **Neville E. Sanjana**[1,2,3,4,*]

[1]New York Genome Center, New York, NY, USA

[2]Department of Biology, New York University, New York, NY, USA

[3]Department of Neuroscience and Physiology, New York University School of Medicine, New York, NY, USA

[4]Perlmutter Cancer Center, New York University School of Medicine, New York, NY, USA

[5]Technology Innovation Lab, New York Genome Center, New York, NY, USA

[6]Department of Biochemistry and Molecular Pharmacology, New York University School of Medicine, New York, NY, USA

Abstract

The engineering of patient T-cells for adoptive cell therapies has revolutionised the treatment of several cancer types[1]. However, further improvements are needed to increase response and cure rates. CRISPR-based loss-of-function screens have been limited to negative regulators of T-cell functions[2-1] and raise safety concerns due to permanent genome modification. Here we identify positive T-cell regulators via overexpression of ~12,000 barcoded human open reading frames (ORFs). The top-ranked genes increased primary human CD4+ and CD8+ T-cell proliferation, activation, and secretion of key cytokines like interleukin-2 and interferon-gamma. In addition, we developed a single-cell genomics method (OverCITE-seq) for high-throughput quantification of the transcriptome and surface antigens in ORF-engineered T-cells. The top-ranked ORF, lymphotoxin beta receptor (LTBR), is typically expressed in myeloid cells but absent

[*]Correspondence: Mateusz Uegut (mateusz.legut@gmail.com), Neville E. Sanjana (neville@sanjanalab.org).
[‡]Present address: Beam Tx, Cambridge, MA, USA
[†]Present address: Immunai, New York, NY, USA

Author contributions

M.L. and N.E.S. designed the study. M.L. performed the screens and validation experiments (including single-cell and CAR work) and analysed data. Z.G. assisted with screens and single-cell data analysis. Z.G., M.G., and X.X. assisted with lentivirus production, T-cell transduction, cell culture and flow cytometry. Z.D. and L.L. performed western blots. J.A.R. assisted with screen and ATAC-seq analyses. C.L. assisted with ATAC-seq. E.P.M., S.H. and P.S. assisted with single-cell experiments. T.D. contributed reagents. C.D. contributed patient samples. M.L. and N.E.S. wrote the manuscript with input from all authors. N.E.S. supervised the study.

Competing interests

The New York Genome Center and New York University have applied for patents relating to the screening methods, identified targets, and OverCITE-seq. C.D. receives research funding from Fate Therapeutics and Bristol Myers Squibb. N.E.S. is an adviser to Vertex and Qiagen.

Reporting summary

Further information on research design is available in the Nature Research Reporting Summary linked to this paper.

in lymphocytes. When overexpressed in T-cells, LTBR induced profound transcriptional and epigenomic remodelling, increasing T-cell effector functions, as well as resistance to exhaustion in chronic stimulation settings, via constitutive activation of the canonical NF-κB pathway. LTBR and other top-ranked genes improved antigen-specific chimeric antigen receptor (CAR) T-cell and γδ T-cell responses, highlighting their potential for future cancer-agnostic therapies[5]. Our results provide several strategies for improving next generation T-cell therapies via induction of new synthetic cell programmes.

Cellular immunotherapies with engineered autologous patient T-cells redirected against a chosen tumour antigen have yielded great efficacy against blood cancers, resulting in five FDA approvals for chimeric antigen receptors (CARs) to date[6]. In contrast, CAR therapy for solid tumours has shown overall much lower efficacy, due to suppression of T-cell effector function in the tumour microenvironment. Even for blood malignancies, outside of B acute lymphoblastic leukaemia, the majority of patients do not experience durable response, with resistance primarily due to T-cell dysfunction rather than antigen loss[7]. Considerable efforts have been devoted to identification of genes and pathways that contribute to T-cell dysfunction[8,9]. However, comprehensive, genome-wide screens for modulators of T-cell function thus far have been limited to loss-of-function[2-4].

The advances in CRISPR genome engineering have made it possible to readily knock out every gene in the genome in a scalable and customizable manner. While its large size makes it challenging, albeit not impossible[10], to deliver Cas9 via lentivirus to primary T-cells, alternative approaches have been developed, reliant on transient delivery of Cas9 protein[2] or mRNA[11], or on constitutive Cas9 expression in engineered isogenic mouse strains[3]. These approaches, however, are not amenable to gain-of-function screens in human cells which require continuous expression of the transcriptional activator driving target gene expression. The large size and immunogenicity of most Cas9-transcriptional activators fusion proteins have limited their utility in T-cell engineering for *in vivo* or clinical approaches[12].

Here, we perform a genome-scale gain-of-function screen in primary human CD4+ and CD8+ T-cells, using a lentiviral library of barcoded human open reading frames (ORFs). We show that T-cells with the strongest proliferation phenotypes are enriched for both known and unknown regulators of the immune response, many of which are not typically expressed by peripheral T-cells. We validated top-ranked ORFs in cells from screen-independent donors and further demonstrate that these ORFs not only drive T-cell proliferation but also increase expression of activation markers and secretion of key proinflammatory cytokines. To gain more comprehensive insight into the mechanism of action of these genes, we developed a single cell sequencing approach coupled with direct ORF capture. We identified lymphotoxin beta receptor (LTBR), one of the top-ranked ORFs not expressed by lymphocytes, as a key driver of profound transcriptional and epigenetic remodelling via increased NF-κB signalling, resulting in a striking increase in proinflammatory cytokine secretion and resistance to apoptosis. Finally, we demonstrated that top-ranked ORFs potentiate antigen-specific T-cell functions, in the context of CD19-directed CAR T-cells and broadly tumour-reactive γδ T-cells from healthy donors and blood cancer patients.

Genome-scale ORF screen in T-cells

In order to avoid relying on constitutive expression of large bacterial proteins or chromatin accessibility in the vicinity of target genes[13], we decided to use a lentiviral library of human open reading frames (ORFs), containing nearly 12,000 full length genes, with ~6 barcodes per gene[14] (Fig. 1a, Extended Data Fig. 1a-g). To date, genome-scale loss-of-function screens in human T-cells focused on either CD4+ or CD8+ T-cells. However, both CD4+ and CD8+ are required for durable tumour control in adoptive therapies[15,16], further exemplified by recent FDA approvals of anti-CD19 CARs with a defined 1:1 CD4+ and CD8+ ratio[1]. Thus, we decided to use the ORF library to discover genes that boost proliferation of both CD4+ and CD8+ T-cells in response to TCR stimulation (Fig. 1a, Extended Data Fig. 1h-j).

We transduced the lentiviral ORF library into CD4+ and CD8+ T-cells from three healthy donors, and, after a brief period in culture (14 days), we re-stimulated the cells to identify drivers of proliferation in response to TCR stimulation. We were able to capture the majority of individual ORF barcodes, and nearly all ORFs, even the largest ones (Extended Data Fig. 1k,l). Comparing the relative frequencies of genes in the most highly proliferative cells to unsorted cells, we found an enrichment of genes known to participate in immune processes among the top-ranked ORFs (Extended Data Fig. 1m,n). We identified *MAPK3* (encoding ERK1), a critical mediator of T-cell functions[17], co-stimulatory molecule CD59[18], transcription factor BATF, and cytokines known to promote T-cell proliferation such as IL12B and IL23A[19]. In fact, two recent studies showed that overexpression of IL12B and BATF boosts proliferation, cytotoxicity and cytokine secretion in CAR T-cells[19,20].

Each ORF in the library is linked to an average of 6 DNA barcodes (Extended Data Fig. 1b). To increase confidence in our top-ranked ORFs from the pooled screen, we assessed the enrichment of individual barcodes corresponding to a given ORF in proliferating CD4+ and CD8+ cells (Fig. 1b,c, Extended Data Fig. 1o). For the majority of ORFs, multiple individual barcodes for each gene were enriched in the highly proliferating population, thus suggesting that the observed enrichment does not stem from spurious clonal outgrowth or PCR bias. To our surprise, the most significantly enriched gene turned out to be lymphotoxin beta receptor (LTBR), a gene broadly expressed on stromal and myeloid cells but completely absent in lymphocytes.

Overall, the enriched ORFs spanned a range of diverse biological processes. Among the top-enriched Gene Ontology (GO) biological processes were lymphocyte proliferation, interferon-gamma (IFNγ) production and nuclear factor kappa-light-chain-enhancer of activated B cells (NF-κB) signalling (Extended Data Fig. 1p). We observed that genes selected by the screen showed only a slight preference for genes endogenously upregulated by T-cells in CD3/CD28 stimulation but in fact were represented in all classes of differential expression (Extended Data Fig. 1q). This result highlights the ability of the pooled ORF screen to discover genes that enable T-cell proliferation but are not expressed normally during CD3/CD28 activation and proliferation. For subsequent validation, we decided to test a broad range of ORFs that function in diverse pathways of relevance to T-cell fitness, and that showed different modes of endogenous regulation (Fig. 1d).

Top ORFs enhance T-cell functions

In order to validate the top-ranked ORFs and understand their impact on other relevant aspects of T-cell function, we sub-cloned 33 ORFs from the library into a vector co-expressing a P2A-linked puromycin resistance gene from the same promoter. We chose a truncated nerve growth factor receptor (tNGFR), lacking its intracellular domain, as a control gene which has no effect on T-cell phenotype[21]. CD4+ and CD8+ populations were separately isolated from several screen-independent healthy donors and transduced with individual ORFs (Fig. 2a). Using flow cytometry on representative ORFs, we confirmed that they were stably and uniformly expressed in both T-cell subsets for the duration of the experiment (Extended Data Fig. 2a,b).

After 14 days post-isolation, we restimulated the cells and measured the relative increase in cell numbers. We found that 16 tested ORFs significantly improved cell proliferation compared with tNGFR, and that proliferation was well correlated between CD4+ and CD8+ cells ($r_s = 0.61$, $p = 0.002$) (Fig. 2b,c, Extended Data Fig. 2c-h). Having established that the top ORFs improve T-cell proliferation, we next tested if there is also a change in other T-cell phenotypes and functions, such as increased cell cycle entry, expression of activation markers IL2RA (CD25) and CD40L (CD 154), and cytokine secretion. The majority of ORFs tested showed no difference in cycling (Extended Data Fig. 2i,j) but showed higher expression of both CD25 and CD154 in T-cells after stimulation (Fig. 2d, Extended Data Fig. 3a), further corroborating their effect on improving the magnitude of T-cell response.

Finally, we measured the secretion of cytokines interleukin (IL)-2 and IFNγ following CD3/CD28 restimulation (Fig. 2e, Extended Data Fig. 3b-e). While our screen was not designed to identify genes that modulate cytokine secretion, several ORFs could both improve T-cell proliferation and boost IL-2 or IFNγ secretion (Fig. 2f). The strongest effect was observed for LTBR which increased secretion of both cytokines in CD4+ and CD8+ T-cells more than 5-fold.

Single-cell analysis of ORF phenotypes

Building on our quantification of how each ORF impacts proliferation, activation and cytokine release, we next sought to better understand the underlying mechanisms driving these changes in cell state. To gain a more comprehensive view of the mechanisms of action of individual ORFs, and to provide a multidimensional description of the phenotypic changes they induce, we developed a single-cell sequencing strategy with direct ORF capture. This approach, OverCITE-seq (**Over**expression-compatible **C**ellular **I**ndexing of **T**ranscriptomes and **E**pitopes by **seq**uencing) builds on previous approaches we have developed for quantifying surface antigens[22] and CRISPR perturbations[23] and allows for high-throughput, single-cell analysis of a pool of T-cells with different ORFs. In brief, mRNA from lentivirally integrated ORFs is reverse transcribed by a primer binding to a constant sequence of the transcript downstream of the ORF and barcoded, along with the cell transcriptome, during template switching. The resulting cDNA pool is then split for separate construction of gene expression and ORF expression libraries (Fig. 3a,b, Extended Data Fig. 4a).

We optimised and applied OverCITE-seq to a pool of ~30 ORFs transduced into CD8+ T-cells from a healthy donor. The cell pool was either left unstimulated ("resting") or stimulated with CD3/CD28 antibodies to mimic TCR activation. To gain confidence in the ORF to single cell assignment, we leveraged the fact that the control gene, tNGFR, is expressed on the cell surface and thus can be captured with a DNA-barcoded antibody[23]. The proportion of cells designated as tNGFR positive was consistent when measured by CITE-seq or flow cytometry (Fig. 3c). An analysis of the entire ORF pool demonstrated that single cells assigned with a given ORF had overall the strongest expression of the corresponding gene (Extended Data Fig. 4b-d), indicating that our ORF capture strategy reliably assigned a genetic perturbation to each single cell.

Unsupervised clustering showed clear separation for stimulated and resting T-cells. Within these activation-driven super-clusters we could observe individual clusters associated with a particular cell state or function, such as cell cycle (clusters 1 and 9), macromolecule biosynthesis (cluster 2), type I IFN signalling (cluster 3), cytotoxicity (cluster 6), T-cell activation and proliferation (cluster 10), and stress response and apoptosis (cluster 11) (Fig. 3d). While in many cases multiple ORFs contributed to a given cluster phenotype (Extended Data Fig. 4e), we observed a striking enrichment of two ORFs, CDK1 and CLIC1, in cluster 1, characterised by increased expression of genes responsible for chromosome condensation in preparation for cell cycle (Fig. 3e). An even stronger enrichment was observed for cluster 10 which was almost exclusively composed of cells expressing LTBR.

To investigate the mechanisms of genetic perturbations with the strongest transcriptional changes, we looked at the transcriptomic profiles of CD3/CD28-stimulated ORF T-cells to unstimulated control T-cells (Extended Data Fig. 4f-i). This approach allowed us to identify gene modules that are shared between perturbations or perturbation-specific. For instance, LTBR and CDK1 showed the strongest enrichment of genes involved in RNA metabolism and cell cycle (*CDK4, HSPA8, BTG3*), as well as in the TNF signalling pathway (*TNFAIP3, TRAF1, CD70*). FOSB appeared to drive an opposite programme to LTBR in terms of genes involved in TCR signalling (*CD3D, CD3E, LAPTM5, LAT*), cytokine responses (*GATA3, TNFRSF4*) and the NF-κB pathway (*NFKB2, NFKBIA, UBE2N*). Finally, we determined that the observed phenotypes were a result of a genetic perturbation rather than an outgrowth of a single clone because virtually every single cell expressed a unique TCR clonotype (Extended Data Fig. 4j). This result highlights the utility of OverCITE-seq's multimodal capture approach, yielding each T-cell 's transcriptome, clonotype, cell surface proteome, cell hashing (for treatment/stimulation conditions), and lentiviral ORF identity.

LTBR improves multiple T-cell functions

Having identified LTBR as a strong driver of proinflammatory cytokine secretion (Fig. 2e) and profound transcriptional remodelling (Fig. 3d,e), we decided to investigate its mechanisms of action in more detail. LTBR belongs to tumour necrosis factor receptor superfamily (TNFRSF) and is expressed on a variety of non-immune cell types and on immune cells of myeloid origin but is absent from lymphocytes (Extended Data Fig. 5a,b). Using bulk RNA-sequencing, we compared global gene expression between LTBR and tNGFR transduced cells, with or without TCR stimulation (Fig. 4a,b, Extended Data

Fig. 5c). In addition to upregulation of MHC-I and II genes (*HLA-C, HLA-B, HLA-DPB1, HLA-DPA1, HLA-DRB6*) and transcription factors necessary for MHC-II expression (*RFX5, CIITA*), LTBR cells also expressed the MHC-II invariant chain (encoded by *CD74*). Interestingly, CD74 has recently been shown in B cells to activate the pro-survival NF-κB pathway, in particular via upregulation of antiapoptotic genes *TRAF1* and *BIRC3* (both of which are also upregulated in LTBR overexpressing cells)[24]. Similarly, LTBR cells strongly upregulated BATF3 which was shown to promote CD8+ T-cell survival[25]. We also observed upregulation of JUNB, a transcription factor (TF) involved in IL-2 production[26], and *TCF7* (encoding TCF1), a key TF responsible for T-cell self-renewal[27]. We confirmed the RNA-sequencing results at the protein level (Extended Data Fig. 5d-i). LTBR cells were also more resistant to activation-induced cell death and retained greater functionality after repeated stimulations (Fig. 4c,d, Extended Data Fig. 5j-m)

LTBR signalling in its endogenous context (in myeloid cells) is triggered either by a heterotrimer of lymphotoxin α (LTA) and β (LTB) or by LIGHT (encoded by the *TNFSF14* gene). Since LTA, LTB and LIGHT are expressed by activated T-cells, we sought to elucidate if addition of exogenous LTA or LIGHT could modulate cytokine secretion, differentiation, or proliferation of CD3/CD28-stimulated LTBR-overexpressing T-cells; however, we found no effect of exogenous ligands on LTBR T-cell function (Extended Data Fig. 6a-e). Thus, while LTBR could potentiate TCR-driven T-cell response, it does not drive activation on its own – which would be a potential safety issue and result in loss of antigen specificity of the engineered T-cell response. We also determined that constitutive LTBR presence is required for maintenance of its phenotype but also that there is a substantial lag time between loss of detectable LTBR expression and loss of phenotype (Extended Data Fig. 6f-i), indicating that transient LTBR expression may be a safe avenue into a therapeutic application.

Finally, to identify the key domains of the LTBR protein that drive its activity in T-cells, we designed a series of point or deletion mutants of LTBR (Fig. 4e, Extended Data Fig. 6j). In general, we found that the N-terminus of LTBR was less sensitive to deletions than the C-terminus. Similarly, a partial reduction of the LTBR phenotype was achieved by introducing three alanine point mutations in the key residues for LTA/LTB binding[28] or removal of the signal peptide. Using our C-terminal deletions, we found that a mutant lacking residues 393:435 showed no difference compared with full length LTBR while the deletion of residues 377:435 completely abrogated the LTBR phenotype, despite being expressed at a comparable, if not higher, level (Extended Data Fig. 6k), probably due to the loss of one TRAF2/3/5 binding site[29]. Moreover, a deletion of the self-association domain[30] (324:377) also completely abrogated the phenotype.

LTBR acts via canonical NF-κB in T-cells

LTBR overexpression was shown to induce broad transcriptomic changes in T-cells, accompanied with changes in T-cell function (Fig. 4a,b). Thus, we sought to determine if the perturbations in gene expression in LTBR cells were accompanied by epigenetic alterations, leveraging the Assay for Transposase-Accessible Chromatin by sequencing (ATAC-seq) (Extended Data Fig. 7a-g). Comparing enrichments of specific TF motifs in differentially

accessible chromatin regions, we identified NF-κB-p65 (RelA) as the most enriched TF in LTBR cells (Extended Data Fig. 7h,i). Of note, NF-κB-p65 and NFAT:AP-1 were the two most enriched TFs in open chromatin in stimulated versus resting T-cells (both LTBR and tNGFR), in line with their well-established role in T-cell activation[31] – but only NF-κB-p65 showed strong enrichment in LTBR cells, with and without stimulation (Fig. 4f). This result suggests that LTBR induces a partial T-cell activation state but still requires signal 1 (TCR stimulation) for full activation.

We then decided to investigate changes in protein expression and/or phosphorylation of the members of the NF-κB signalling pathway. We observed a more rapid phosphorylation of p65/RelA and a strong increase in phosphorylation of an NF-κB inhibitor IκBα which targets IκBα for degradation — both of which enhance NF-κB activation/transcription (Fig. 4g,h, Extended Data Fig. 8a-c). In addition to changes in the canonical NF-κB pathway we also detected upregulation of key mediators of the non-canonical NFκB pathway, RelB and NF-κB p52 (Fig. 4i, Extended Data Fig. 8b,c).

Having established that LTBR activates both the canonical and non-canonical NF-κB pathways, we sought to determine the molecular underpinnings of this phenomenon by perturbing key genes in the LTBR/NF-κB pathways via co-delivery of LTBR/tNGFR and CRISPR constructs targeting 11 genes involved in the LTBR signalling pathway[32] (Fig. 4j, Extended Data Fig. 8d-o). Knockout of LTB, TRAF2, and NIK significantly reduces IFNγ secretion from LTBR cells but not (or to lesser extent) from control (tNGFR) cells; while LIGHT, ASK1, and RELA perturbations have a stronger effect on control cells than LTBR cells. The effect of LTB loss on T-cell activation in LTBR cells supports the observation that alanine mutagenesis of key residues involved in LTA/LTB binding (Fig. 4e) partially reduced the LTBR phenotype. Interestingly, we observed that loss of either TRAF2 or TRAF3 boosted IFNγ secretion in tNGFR cells only, in line with previous findings that T cells from TRAF2 dominant negative mice are hyperresponsive to TCR stimulation[33].

To explore the potential roles of canonical versus non-canonical NF-κB signalling in LTBR T-cells, we decided to investigate the global effects of RELA or RELB loss on the LTBR-driven gene expression profiles. Using bulk RNA-sequencing on T cells overexpressing LTBR or tNGFR, we discovered that only RELA loss significantly downregulates the expression of “core” LTBR genes while RELB loss had no effect (Fig. 4k, Extended Data Fig. 8p).

ORFs enhance antigen-specific responses

Thus far we demonstrated that top-ranked genes from the ORF screen improve T-cell function using a non-specific, pan-TCR stimulation. Here, we sought to determine if a similar improvement can be observed using antigen-specific stimulation (Fig. 5a). To that effect, we co-expressed several top-ranked genes with two FDA-approved chimeric antigen receptors targeting CD19, a B-cell marker (Extended Data Fig. 9a-d). Using LTBR as an example, we demonstrated that ORF expression is achievable with this tricistronic vector (Extended Data Fig. 9e-i).

Since both CARs use different costimulatory domains, from CD28 or 4-1BB, we wanted to determine if top-ranked genes selected using CD28 co-stimulation could also work in context of 4-1BB co-stimulation. Nearly all top-ranked genes tested, with exception of *AKR1C4*, improved upregulation of CD25 and antigen-specific cytokine secretion, with no major differences in the differentiation/exhaustion phenotype (Fig. 5b,c, Extended Data Fig. 9j-p, Extended Data Fig. 10a-d).

While production of IL2- and IFNγ is crucial for T-cell clonal expansion and antitumour activity, another vital component of tumour immunosurveillance is direct cytotoxicity. Top-ranked genes had an overall stronger effect on the cytotoxicity of CD28 CAR than 4-1BB CAR (Fig. 5d-f, Extended Data Fig. 10e,f). Interestingly, we observed that CAR T-cells co-expressing LTBR tended to form large cell clusters, typically absent in wells with control cells but in line with overall higher expression of adhesion molecules such as ICAM-1 in LTBR-expressing cells (Extended Data Fig. 10g). Another important feature of effective antitumour T-cells is the ability to maintain functionality despite chronic antigen exposure. In line with our previous findings in context of LTBR alone (Fig. 4d), CAR/LTBR cells showed superior functionality to matched CAR/tNGFR cells after repeated challenge with target cells (Fig. 5g, Extended Data Fig. 10h-j).

T cells from healthy donors are relatively easy to engineer and rarely show signs of dysfunction in culture, while autologous T-cells in cancer patients are often dysfunctional, showing limited proliferation and effector functions[34]. To investigate if top-ranked genes can improve CAR response not only in healthy T-cells but also in potentially dysfunctional patient-derived cells, we transduced CD19 CARs co-expressed with LTBR or a control gene into PBMCs from diffuse large B cell lymphoma patients. Upon co-incubation with CD19+ target cells we observed a similar increase of IL-2 and IFNγ secretion from LTBR CAR T-cells as in healthy donors, indicating that identified ORFs can be successfully used to engineer lymphoma patient T-cells *ex vivo* (Fig. 5h, Extended Data Fig. 10k). Importantly, there was no cytokine secretion in response to $CD19^{neg}$ cells, indicating that LTBR overexpression does not induce spurious, antigen-independent response.

The screen and subsequent validations were performed in αβ T-cells, the predominant subset in human peripheral blood. While αβ T-cell-based immunotherapy has shown tremendous potential in the clinic, γδ T-cells present an attractive alternative, due to their lack of MHC restriction, ability to target broadly expressed stress markers in a cancer type-agnostic manner, and more innate-like characteristics[5]. Here we sought to determine if the top genes validated in αβ T-cells translated to γδ T-cells. Following co-incubation with leukaemia or pancreatic ductal adenocarcinoma cancer cells, we observed an increase in IL-2 and IFNγ secretion from γδ T-cells transduced with top-ranked genes (Fig. 5i, Extended Data Fig. 10l-p). Thus, top-ranked genes from our screen can act on signalling pathways conserved between even highly divergent T-cell subsets, highlighting their broad applicability for cancer immunotherapy.

Discussion

In summary, we developed a genome-scale gain-of-function screen in primary human T-cells, examining the effects of nearly 12,000 full-length genes on TCR-driven proliferation in a massively-parallel fashion. To date, the largest published gain-of-function study in primary T-cells involved 36 constructs, including full-length genes and synthetic receptors[35]. That approach, developed by Marson and colleagues, relied on construct delivery via donor DNA and Cas9-mediated targeted insertion. While using donor DNA for target gene delivery allows for more flexibility in terms of construct design, especially for engineering synthetic receptors, that method is less scalable and less accessible in terms of cost and complexity than the lentiviral library used herein. Thus, we believe that ORF-based gain-of-function screens are readily applicable to a plethora of T-cell phenotypes and settings, as well as offering a path for clinical translation. In fact, all FDA-approved CAR therapies already rely on lenti- or retroviral integration of a CAR transgene, and therefore an addition of an ORF to this system should pose no major manufacturing or regulatory challenges. Use of ORF-encoding mRNA delivered to CAR T-cells prior to infusion is another translational route, especially if there are safety concerns about the mode of action of a particular ORF.

Gain-of-function screens have the potential to uncover regulators that are tightly controlled, restricted to a specific developmental stage, or expressed only in certain circumstances. As demonstrated here, LTBR is canonically absent from cells of lymphoid origin but due to the intact signalling pathway it can play a synthetic role when introduced to T-cells. While constitutive activation of other TNFRSF members might result in a similar phenotype, one of the features that distinguishes LTBR (and plausibly led to its enrichment, but not other TNFRSF members, in the screen) is formation of an autocrine loop whereby the receptor and its ligands are present in the same cell. It is of particular interest that LTBR expression boosts IL-2 secretion since this cytokine is produced exclusively by T-cells and not cell types endogenously expressing LTBR. In addition to boosting cytokine secretion, LTBR overexpression promoted stemness (TCF1 expression) and decreased activation-induced apoptosis, as well as offered a level of protection against phenotypic and functional hallmarks of T-cell exhaustion – all of which are features not recapitulated by cell types endogenously expressing LTBR. Previous work using LTBR overexpression in cell lines demonstrated that LTBR plays a pro-apoptotic role[36], in direct contrast to the phenotype we observed in primary T-cells. Transcript- and protein-level analyses revealed that LTBR drives constitutive activation of both canonical and non-canonical NF-κB pathways. However, using epigenomic profiling and CRISPR-based functional perturbations we demonstrated that the phenotypic and functional changes resulting from LTBR expression are mediated primarily via the canonical NF-κB pathway activation while changes in the non-canonical pathway may not be essential for the observed phenotypes, in contrast to well-established role of non-canonical NF-κB activation in cells that endogenously express LTBR[37].

Gene overexpression has been used for pre-clinical enhancement of CAR T-cell therapies in numerous studies. For instance, armouring CAR T-cells with cytokines such as IL12 or IL18, not typically produced by T-cells but known to improve T-cell function when secreted by other cell types, was shown to improve their anti-tumour activity[38,39]. Notably,

a recent report by Mackall and colleagues demonstrated that CAR T-cell exhaustion can be alleviated by overexpression of c-JUN, a transcription factor identified via RNA-sequencing as specifically depleted in exhausted cells[40]. We believe that armouring CARs with LTBR (full-length or a truncated version) and other top-ranked genes identified here could result in development of a new generation of cellular therapies. We envision further extensions of the screening approach presented here to more sophisticated models, for instance involving co-culture of edited T-cells with antigen-presenting or immunosuppressive cells to identify genes that can modulate cell-cell crosstalk, a crucial feature of the immune response. Future studies adapting genome-wide gain-of-function screens to relevant models of immunotherapy will lead to advanced target selection for engineering novel synthetic cellular therapies that can overcome the immunosuppressive tumour microenvironment and eradicate established cancers.

METHODS

Isolation and culture of primary human T-cells

Regular buffy coats containing peripheral blood from de-identified healthy donors were collected by and purchased from the New York Blood Center under an IRB-exempt protocol. All donors provided informed consent. Peripheral blood mononuclear cells (PBMC) were isolated from buffy coats using Lymphoprep (Stemcell) gradient centrifugation. For most assays, CD8+ and CD4+ were isolated sequentially from the same donor. First, CD8+ T-cells were isolated by magnetic positive selection using EasySep Human CD8 Positive Selection Kit II (Stemcell). Then, CD4+ T-cells were isolated from the resulting flowthrough by negative magnetic selection using EasySep Human CD4+ T-cell Isolation Kit (Stemcell), γδ T-cells were isolated by magnetic negative selection using EasySep Human Gamma/Delta T-cell Isolation Kit (Stemcell). Immediately after isolation T-cells were resuspended in T-cell Media, which consisted of Immunocult-XF T-cell Expansion Medium (Stemcell) supplemented with 10 ng mL^{-1} recombinant human IL-2 (Stemcell).

Activation of T cells was performed with Immunocult Human CD3/CD28 T-cell Activator (Stemcell) using 25 μl per 10^6 cells per mL. Typically, T-cells were transduced with concentrated lentivirus 24 h post isolation. For some experiments, T-cells were electroporated with *in vitro* transcribed mRNA 24 h post isolation or with Cas9 protein 48 h post isolation. 72 h post isolation, lentivirally transduced T-cells were selected with 2 μg mL^{-1} puromycin.

Every 2-3 days T-cells were either split or had media replaced to maintain cell density of 1-2 × 10^6 cells per mL. Lentivirally transduced T-cells were maintained in media containing 2 μg mL^{-1} puromycin for the duration of culture. T-cells were used for phenotypic or functional assays between 14 and 21 days post isolation, or cryopreserved in Bambanker Cell Freezing Media (Bulldog Bio), γδ T-cells were further purified prior to functional assays using anti-Vγ9 PE antibody (Biolegend) and anti-PE Microbeads (Miltenyi Biotec) according to manufacturer's recommendations, in presence of dasatinib, a protein kinase inhibitor to prevent from activation-induced cell death resulting from TCR crosslinking[42]. Peripheral blood mononuclear cells from patients with diffuse large B cell lymphoma were

obtained from the Perlmutter Cancer Center under a Perlmutter Cancer Center Institutional Review Board approved protocol (S14-02164).

Vector design and molecular cloning

All vectors used were cloned using Gibson Assembly (NEB). For experiments shown in Figure 1, we used the lentiviral backbone from the pHAGE plasmid[14]. For all other experiments, the backbone from lentiCRISPRv2 (Addgene 52961) was used. ORFs were PCR amplified for cloning from the genome-scale library used in the screen.

After adding Gibson overhangs by PCR, ORFs and P2A-puro were inserted into *Xba*I and *Eco*RI cut lentiCRISPRv2. The sgRNA cassette was removed from lentiCRISPRv2 using *Pac*I and *Nhe*I digest. For LTBR overexpression and knockout experiments, the sgRNA cassette was not removed. CARs were synthesized as gBlocks (IDT). For CAR-ORF cloning, CAR-P2A-puro-T2A(partial) were first inserted into *Xba*I and *Eco*RI cut lentiCRISPRv2. For subsequent ORF insertion, the plasmid was cut with *Hpa*I located within the partial T2A and *Eco*RI. The following vectors were deposited to Addgene: pOT_01 (lenti-EFS-LTBR-2A-puro, Addgene 181970), pOT_02 (lenti-EFS-tNGFR-2A-puro, Addgene 181971), pOT_03 (lenti-EFS-FMC6.3-28z-2A-puro-2A-LTBR, Addgene 181972), pOT_04 (lenti-EFS-FMC6.3-BBz-2A-puro-2A-LTBR, Addgene 181973), pOT_05 (lenti-EFS-FMC6.3-28z-2A-puro-2A-tNGFR, Addgene 181974), pOT_06 (lenti-EFS-FMC6.3-BBz-2A-puro-2A-tNGFR, Addgene 181975).

Nuclease and CRISPR guide RNA design

All sgRNAs were designed using the GUIDES webtool[43]. We selected guides targeting initial protein-coding exons (with the preference for targeting protein family domains enabled in GUIDES) as well as minimising off-target and maximising on-target scores. For Cas9 nuclease nucleofection, we used purified sNLS-SpCas9-sNLS nuclease (Aldevron).

Preparation of ORF library plasmids for paired-end sequencing

We re-amplified a previously described genome-scale ORF library[14] using Endura electrocompetent cells (Lucigen). The identity of ORFs and matched barcodes was confirmed by paired-end sequencing. In brief, the plasmid was first linearised with I-*Sce*I meganuclease, which cuts downstream of the barcode. Then, the linearised plasmid was tagmented using TnY transposase[44]. Then, the fragmented plasmid was amplified in a PCR reaction, using a forward primer binding to a handle introduced by TnY and a reverse primer binding to a sequence downstream of the barcode. All transposons and PCR primer oligonucleotides were synthesized by IDT (Supplementary Table 2). The resulting amplicon was sequenced on a NextSeq 500. The forward read (containing the ORF) was mapped to GRCh38.101 CDS transcriptome annotations using star 2.7.3a (map quality ≥ 10)[45]. Using the paired end read, we also captured the 24 nucleotide barcode downstream of the constant plasmid sequence. We tabulated ORF-barcode combinations and further curated this table by eliminating any spurious pairs that might be due to sequencing or PCR error. Specifically, a permutation test was performed to identify the maximum number of ORF-barcode combinations expected by random chance, after which we only kept ORF-barcode combinations whose count exceeded this maximum number. We excluded all non-coding

elements from the reference and then collapsed barcodes that were within a Levenshtein distance less than 2.

Cell culture

HEK293FT cells were obtained from Thermo Fisher and cultured in DMEM supplemented with 10% Serum Plus-II (Thermo Fisher). Nalm6, Jurkat and BxPC3 cells were obtained from ATCC and cultured in RPMI-1640 supplemented with 10% Serum Plus-II. Capan2 cells were obtained from ATCC and cultured in McCoy's Medium supplemented with 10% Serum Plus-II. For γδ co-incubation experiments, cell lines were pre-treated with 50 μM zoledronic acid (Sigma) for 24h. Cell lines were routinely tested for mycoplasma using MycoAlert PLUS (Lonza) and found to be negative. Cell lines have not been authenticated in this study.

Lentivirus production

We produced lentivirus by co-transfecting third-generation lentiviral transfer plasmids together with packaging plasmid psPAX2 (Addgene 12260) and envelope plasmid pMD2.G (Addgene 12259) into HEK293FT cells, using polyethyleneimine linear MW 25000 (Polysciences). After 72 hours, we harvested the supernatants, filtered them through a 0.45 μm Steriflip-HV filter (Millipore), and concentrated the virus using Lentivirus Precipitation Solution (Alstem). Concentrated lentivirus was resuspended in T-cell Media containing IL-2 and stored at −80C.

Pooled ORF library screening

For pooled ORF library screening, CD4+ and CD8+ T-cells were isolated from a minimum of 500 x 10^6 PBMC from three healthy donors. The amount of lentivirus used for transduction was titrated to result in 20-30% transduction efficiency, to minimize the probability of multiple ORFs being introduced into a single cell. The cells were maintained in T-cell media containing 2 μg mL^{-1} puromycin and counted every 2-3 days to maintain cell density of 1-2 x 10^6 cells mL^{-1}. On day 14 after isolation, T-cells were harvested, counted, labelled with 5 μM carboxyfluorescein succinimidyl ester (CFSE) (Biolegend) and stimulated with CD3/CD28 Activator (StemCell) at 1.56 μL per 1 x 10^6 cells. An aliquot of cells representing 1,000X coverage of the library was frozen down at this step to be used as a pre-stimulation control. After 4 days of stimulation, cells were harvested and an aliquot of cells representing 1,000X coverage of the library was frozen down to be used as a pre-sort control. The remaining cells were stained with LIVE/DEAD Violet cell viability dye (Thermo Fisher), and $CFSE^{low}$ cells (corresponding to the bottom 15% of the distribution) were sorted using Sony SH800S cell sorter. Genomic DNA was isolated, and two rounds of PCR to amplify ORF barcodes and add Illumina adaptors were performed[46] (Supplementary Table 2).

Pooled ORF screen analysis

For most of the analyses, equal numbers of reads from all three donors were combined per bin before trimming and alignment. The barcodes were mapped to the reference library after adaptor trimming with `cutadapt` 1.13 (`-m 24 -e 0.1 --discard-untrimmed`)

using `bowtie` 1.1.2 (`-v 1 -m 1 --best --strata`)[47,48]. All subsequent analyses were performed in `RStudio` 1.1.419 with `R` 4.0.0.2. To calculate individual barcode enrichment, barcode counts were normalised to the total number of reads per sample (with pseudocount added) and $\log_2$ transformed. To calculate ORF enrichment, raw barcode counts were first collapsed by genes before normalisation and $\log_2$ transformation.

We performed enrichment analyses at both the barcode- and gene-level. Statistical analysis on barcode enrichment was performed using `MAGeCK`[49], comparing $CFSE^{low}$ samples to corresponding inputs (pre-stimulation), using CD4+ and CD8+ as replicates. Statistical analysis on ORF enrichment was performed using `DESeq2`[50]. We obtained raw gene counts by collapsing barcodes into corresponding genes. $CFSE^{low}$ samples were compared to corresponding inputs (both pre-stimulation and pre-sort), using CD4+ and CD8+ as replicates. Gene ontology enrichment (biological process) on genes passing `DESeq2` criteria ($\log_2$[fold-change] > 0.5, $p_{adj.} < 0.05$) was performed using the topGO package[51]. For the genes enriched in the $CFSE^{low}$ screen (`DESeq2` analysis), we overlapped these genes with differentially-expressed genes after CD3/CD28 stimulation using data from the Database of Immune Cell Expression (DICE: https://dice-database.org/)[41]. For differentially-expressed genes, we used the following DICE datasets: “T cell, CD4, naive” vs. “T cell, CD4, naive [activated]”, “T cell, CD8, naive” vs. “T cell, CD8, naive [activated]”. Significant differential expression was as given in the DICE dataset ($p_{adj} < 0.05$).

Proliferation assays

Transduced T-cells were harvested at day 14 after isolation, counted and plated at 2.5 x 10^4 cells per well in a round bottom 96-well plate, in two sets of triplicate wells per transduction. One set of triplicate wells was cultured in Immunocult-XF T-cell Expansion Medium supplemented with 10 ng mL^{-1} IL-2 and another set of triplicate wells was further supplemented with 1.56 µl CD3/CD28 Activator per 1 mL of media. The cells were cultured for 4 days, and then were harvested and stained with LIVE/DEAD Violet cell viability dye. Prior to flow cytometric acquisition, the cells were resuspended in D-PBS with 10% v/v Precision Counting Beads (Biolegend). For quantification, the number of viable cell events was normalised to the number of bead events per sample. Then, for each ORF the normalised number of viable cells in wells supplemented with CD3/CD28 Activator was divided by the mean number of viable cells in control wells to quantify T-cell proliferation. To enable comparisons between donors and CD4+/CD8+ T-cells, proliferation of T-cells transduced with a given ORF was finally normalised to proliferation of matched tNGFR control.

In addition to the counting beads assay, we also measured proliferation using a dye dilution assay. For this assay, transduced T-cells were harvested at day 14 post-isolation, washed with D-PBS, and then labelled with 5 µM CellTrace Yellow (CTY) in D-PBS for 20 min at room temperature. The excess dye was removed by washing with 5-fold excess of RPMI-1640 supplemented with 10% Serum Plus-II. The labelled cells were then plated at 2.5 x 10^4 cells per well on a round bottom 96-well plate. One set of triplicate wells was cultured in unsupplemented Immunocult-XF T-cell Expansion Medium (i.e. without IL-2) and another set of triplicate wells was supplemented with 10 ng mL^{-1} IL-2 and 1.56 µl

CD3/CD28 Activator per 1 mL of media. The cells were cultured for 4 days, and then were harvested and stained with LIVE/DEAD Violet cell viability dye. For quantification of the proliferation index, events were first gated on viable T-cells in FlowJo (Treestar) and exported for further analysis in R/RStudio using `flowfit` and `flowcore` packages[52]. Unstimulated cells were used to determine the parent population size and position to account for differences in staining intensity between different samples. These fitted parent population parameters were then used to fit the CTY profiles of matched stimulated samples, modelled as Gaussian distributions assuming $\log_2$ distanced peaks as a result of cell division and dye dilution. Fitted CTY profiles were inspected visually for concordance with the original CTY profiles and used to calculate the proliferation index. The proliferation index is defined as the sum of cells in all generations divided by the computed number of parent cells present at the beginning of the assay.

Flow cytometry for cell surface and intracellular markers

All antibodies and dyes used for flow cytometry are listed in Supplementary Table 3. For CD25 (IL2RA) and CD154 (CD40L) quantification, T-cells were re-stimulated with CD3/CD28 Activator (6.25 μl per 10^6 cells) for 6 hours (CD154 staining in CD8+) or for 24 hours prior to staining (CD25 staining in both CD4+ and CD8+, and CD154 staining in CD4+). For Ki-67 and 7-AAD staining, T-cells were rested overnight in Immunocult-XF T-cell Expansion Medium without IL-2 and then activated with CD3/CD28 Activator (25 μl per 10^6 cells) for 24 hours. In other cases, T-cells were stained without stimulation. For detection of secreted proteins, T-cells were stimulated for 24 hours with CD3/CD28 Activator (25 μl per 10^6 cells) (LTA, LIGHT), and protein transport inhibitors brefeldin A (5 μg/mL) and monensin (2 μM) were included for the last 6 hours of stimulation (IL12B, LTA, LIGHT).

First, the cells were harvested, washed with D-PBS and stained with LIVE/DEAD Violet cell viability dye for 5 minutes at room temperature in the dark, followed by surface antibody staining for 20 minutes on ice. After surface antibody staining (where applicable) the cells were washed with PBS and acquired on Sony SH800S cell sorter or taken for intracellular staining. For intracellular staining, the cells were resuspended in an appropriate fixation buffer. The following fixation buffers were used for specific protein detection: Fixation Buffer (Biolegend) for IL12B and MS4A3 staining; True-Nuclear Transcription Factor Fix (Biolegend) for BATF, TCF1, and FLAG staining; FoxP3/Transcription Factor Fixation Reagent, (eBioscience) for Ki-67. After resuspension in the fixation buffer, cells were incubated at room temperature in the dark for 1 hour. Following the incubation, the cells were washed twice in the appropriate permeabilization buffer. The following permeabilization buffers were used: Intracellular Staining Permeabilization Wash Buffer (Biolegend) for IL12B and MS4A3 staining; True-Nuclear Perm Buffer (Biolegend) for BATF, TCF1, and FLAG staining; FoxP3/Transcription Factor Permeabilization Buffer (eBioscience) for Ki-67. After permeabilization, the cells were stained with the specific antibody or isotype control for 30 minutes in the dark at room temperature. Finally, the cells were washed twice in the appropriate permeabilization buffer and acquired on a Sony SH800S flow cytometer. For cell cycle analysis, the cells were further stained with 0.5 μg/mL 7-amino-actinomycin D (7-AAD) for 5 minutes immediately before acquisition.

Gating was performed using appropriate isotype, fluorescence minus one and biological controls. Typically, 5,000-10,000 live events were recorded per sample.

Flow cytometry detection of phosphorylated proteins

T-cells were rested for 24 hours in in Immunocult-XF T-cell Expansion Medium without IL-2 prior to detection of phosphorylated proteins. The rested cells were stimulated with CD3/CD28 Activator (25 μl per 10^6 cells) for times indicated in the corresponding figure. Immediately after the stimulation period the cells were fixed with a 1:1 volume ratio of the pre-warmed Fixation Buffer (Biolegend) for 15 minutes at 37°C and washed twice with the cell staining buffer (D-PBS + 2% FBS). As per the manufacturer's protocol, the cells were resuspended in the residual volume and permeabilised in 1 mL of pre-chilled True-Phos Perm Buffer (Biolegend) while vortexing. The cells were incubated in the True-Phos Perm Buffer for 60 minutes at −20°C. After permeabilization the cells were washed twice with the cell staining buffer and stained with anti-CD4, anti-CD8, anti-RelA and anti-phospho-RelA antibodies (or isotype controls) for 30 minutes at room temperature. Following staining, the cells were washed twice in the cell staining buffer and acquired on Sony SH800S cell sorter. Gating was performed on CD4+ or CD8+ cells, and the levels of RelA and phospho-RelA were determined using appropriate isotype and biological controls.

Western blot detection of proteins and phosphorylated proteins

T-cells expressing tNGFR or LTBR, resting or stimulated for 15 minutes with CD3/CD28 Activator (25 μl per 10^6 cells), were collected, washed with 1x D-PBS and lysed with TNE buffer (10 mM Tris-HCl, pH 7.4, 150 mM NaCl, 1mM EDTA, 1% Nonidet P-40) in the presence of a protease inhibitor cocktail (Bimake B14001) and a phosphatase inhibitor cocktail (Cell Signaling Technologies 5872S) for 1 hour on ice. Cells lysates were spun for 10 minutes at 10,000 g, and the protein concentration was determined with the BCA assay (Thermo). Equal amounts of cell lysates (25 mg) were denatured in Tris-Glycine SDS Sample buffer (Thermo) and loaded on a Novex 4-12 or 4-20 % Tris-Glycine gel (Thermo). The PageRuler pre-stained protein ladder (Thermo) was used to determine the protein size. The gel was run in 1x Tris-Glycine-SDS buffer (IBI Scientific) for about 120 min at 120V. Proteins were transferred on a nitrocellulose membrane (BioRad) in the presence of prechilled 1x Tris-Glycine transfer buffer (Fisher Scientific) supplemented with 20% methanol for 100 min at 100V.

Immunoblots were blocked with 5% skim milk dissolved in 1x PBS with 1% Tween-20 (PBST) and incubated overnight at 4°C separately with the following primary antibodies: rabbit anti-GAPDH (0.1 mg/mL, Cell Signaling, 2118S), mouse anti-IKKα (1:1000 dilution, Cell Signaling, 3G12), rabbit anti-IKKβ (1:1000 dilution, Cell Signaling, D30C6), rabbit anti-NF-κB p65 (1:1000 dilution, Cell Signaling, D14E12), rabbit anti-phospho-NF-κB p65 Ser536 (1:1000 dilution, Cell Signaling, 93H1), mouse anti-IκBα (1:1000 dilution, Cell Signaling, L35A5), rabbit anti-phospho-IκBα Ser32 (1:1000 dilution, Cell Signaling, 14D4), rabbit anti-NF-κB p100/p52 (1:1000 dilution, Cell Signaling, 4882), and rabbit anti-RelB (1:1000 dilution, Cell Signaling, C1E4). Following the primary antibody, the blots were incubated with IRDye 680RD donkey anti-rabbit (0.2 mg/mL, LI-COR 926-68073) or with IRDye 800CW donkey anti-mouse (0.2 mg/mL, LI-COR 926-32212). The blots were

imaged using Odyssey CLx (LI-COR) and quantified using ImageJ v1.52. The uncropped and unprocessed blots are shown in Supplementary Figure 1.

Quantification of cytokine secretion

For measurement of secreted IFNγ and IL-2, T-cells were first harvested and rested for 24 hours in media without IL-2. Then, they were counted, plated at 2.5 x 10^4 cells per well in a round bottom 96-well plate and incubated in media without IL-2, with or without CD3/CD28 Activator (25 μl per 10^6 cells) for 24h. Then, cell supernatants were harvested, diluted and used for cytokine quantification via enzyme-linked immunosorbent assay (Human IL-2 or IFNγ DuoSet, R&D Systems) using an Infinite F200 Pro (Tecan) plate reader. Multiplexed quantification of secreted cytokines and chemokines in resting or stimulated T-cells was performed using the Human Cytokine/Chemokine 48-Plex Discovery Assay Array (Eve Technologies).

T cell killing assays

CD19+ Nalm6 cells were first transduced with a lentiviral vector encoding EGFPd2PEST-NLS and puromycin resistance gene[53]. The transduced cells were kept in puromycin selection throughout the culture, to maintain stable EGFP expression, and puromycin was only removed from the media prior to the killing assay. T-cells were transduced with a vector encoding a chimeric antigen receptor specific for CD19, using either a CD28 stalk, CD28 transmembrane and CD28 signalling domain or CD8 stalk and CD8 transmembrane domain with 4-1BB signalling domain, and CD3ζ signalling domain[54]. 14 days after transduction, transduced T-cells were combined with 5 x 10^4 Nalm6 GFP+ cells in triplicate at indicated effector:target ratios in a flat 96-well plate pre-coated with 0.01% poly-L-ornithine (EMD Millipore) in Immunocult media without IL-2. The wells were then imaged using an Incucyte SX1, using 20X magnification and acquiring four images per well every 2 hours for up to 120 hours. For each well, the integrated GFP intensity was normalised to the 2 hour timepoint, to allow the cells to fully settle after plating.

In vitro mRNA preparation

The template for *in vitro* transcription was generated by PCR from a plasmid encoding LTBR or tNGFR with the resulting amplicon including a T7 promoter upstream of the ORF (Supplementary Table 2). The purified template was then used for *in vitro* transcription with capping and poly-A tailing using the HiScribe T7 ARCA mRNA Kit with Capping (NEB).

Primary T-cell nucleofection

Activated T-cells were nucleofected with *in vitro* transcribed mRNA at 24 hours post-activation or with Cas9 protein at 48 hours post-activation. The cells were harvested, washed 2X in PBS and resuspended in P3 Primary Cell Nucleofector Solution (Lonza) at 5 x 10^5 cells per 20 μL. Immediately after resuspension, 1 μg mRNA or 10 μg Cas9 (Aldevron) were added (not exceeding 10% v/v of the reaction) and the cells were nucleofected using the E0-115 program on a 4D-Nucleofector (Lonza). After nucleofection the cells were resuspended in pre-warmed Immunocult media with IL-2 and recovered at 37°C with 5%

CO_2 for 20 min. After recovery the cells were plated at 1 x 10^6 cells per mL and used in downstream assays.

OverCITE-seq sample preparation and sequencing

For single cell sequencing, CD8+ T-cells were individually transduced with ORFs and kept, separately, under puromycin selection for 14 days. Then, transduced cells were combined and split into two conditions: one was cultured for 24 hours only in presence of IL-2, the other was further supplemented with 6.25 μl CD3/CD28 Activator per 10^6 cells. After stimulation, the cells were harvested, counted and resuspended in staining buffer (2% BSA + 0.01% Tween-20 in PBS) at 2 x 10^7 cells per mL. Then, 10% (v/v) Human TruStain FcX Fc Receptor Blocking Solution (Biolegend) was added and the cells were incubated at 4C for 10 min. After Fc receptor blocking, the cell concentration was adjusted to 5 x 10^6 cells per mL and the stimulated and unstimulated cells were split into 4 conditions each. Each condition received a different oligonucleotide-conjugated (barcoded) cell hashing antibody to allow for pooling of different conditions in the same 10x Genomics Chromium lane[23]. After 20 min co-incubation on ice, the cells were washed 3X with staining buffer and counted using Trypan blue exclusion. Cell viability was typically ~95%.

Then, cells stained with different hashing antibodies were pooled together at equal numbers and stained with the following oligonucleotide-conjugated (barcoded) antibodies for quantification of cell surface antigens: CD11c (0.1 μg), CD14 (0.2 μg), CD16 (0.1 μg), CD19 (0.1 μg), CD56 (0.2 μg), CD3 (0.2 μg), CD45 (0.01 μg), CD45RA (0.2 μg), CD45RO (0.2 μg), CD4 (0.1 μg), CD8 (0.1 μg), CD25 (0.25 μg), CD69 (0.25 μg), NGFR (0.25 μg) (TotalSeq-C, Biolegend). The cells were stained for 30 min on ice, washed 3X with staining buffer, resuspended in PBS and filtered through 40 μm cell strainer. The cells were then counted and the concentration was adjusted to 1 x 10^6 mL^{-1}. For loading into the 10x Genomics Chromium, 3 x 10^4 cells were combined with Chromium Next GEM Single Cell 5' v2 Master Mix (10x Genomics) supplemented with a custom reverse primer binding to the puromycin resistance cassette for boosting ORF transcript capture at the reverse transcription stage (Supplementary Table 2). The custom reverse primer was added at 1:3 ratio to poly-dT primer included in the Master Mix.

For cDNA amplification, additive primers for amplification of sample hashing and surface antigen barcodes were included[23], as well as a nested reverse primer binding to the puromycin resistance cassette downstream of the ORF. Following cDNA amplification, SPRI beads were used for size selection of resulting PCR products – small size (<300 bp) sample hashing and surface antigen barcodes were physically separated from larger cDNA and ORF amplicons for downstream processing. Sample hashing and surface antigen barcodes were also processed [22]. Amplified cDNA was then separated into three conditions, for construction of the gene expression library, αβ TCR library and ORF library. The ORF library was processed similarly to αβ TCR library, using nested reverse primers binding downstream of the ORF (Supplementary Table 2). The quality of produced libraries was verified on BioAnalyzer using High Sensitivity DNA kit (Agilent). The libraries were sequenced on NextSeq 500. For the gene expression library, >25,000 reads per cell were generated. For other libraries, >5,000 reads per cell were generated.

OverCITE-seq data analysis

Gene expression unique molecular identifier (UMI) count matrices and TCR clonotypes were derived using 10X Genomics Cell Ranger 3.1.0. HTO and antibody UMI count matrices were generated using `kallisto` 0.46.0[55] and `bustools` 0.39.3[56]. ORF reads were first aligned to plasmid references using `bowtie2` 2.2.8[57] and indexed to the associated ORF, after which `kallisto` and `bustools` were used to generate UMI count matrices. All modalities were normalised using a centred log ratio (CLR) transformation. Cell doublets and negatives were identified using the `HTODemux`[58] function and then excluded from downstream analysis. The UMI cutoff quantile for `HTODemux` was optimised to maximize singlet recovery using grid search with values between 0 and 1. ORF singlets were identified using `MULTIseqDemux`[59]. We then excluded cells with low quality gene expression metrics and removed cells with less than 200 unique RNA features or greater than 5% of reads mapping to the mitochondrial transcriptome.

Count matrices were then loaded into and analysed with `Seurat` 4.0.1[60]. Cell cycle correction and scaling of gene expression data was performed using the `CellCycleScoring` function with default genes followed by scaling the data using the ScaleData function. Principal component (PC) optimization of the scaled and corrected data was then performed using `Jackstraw`[61] where we selected all PCs up to the first non-significant PC to use in clustering. Clustering of cells was performed using a shared nearest neighbour (SNN)-based clustering algorithm and visualised using UMAP dimensional reduction[62] to project cluster PCs into 2D space. Cluster marker analysis was performed using the `FindAllMarkers` with the hypothesis set defined as positive and negative markers present in at least 25% of cluster cells and with a $\log_2$-fold-change threshold of 0.25 as compared to non-cluster cells. Differential expression (DE) analysis of ORFs was performed using `DESeq2`[50] to identify genes up and downregulated in ORF expressing cells as compared to NGFR (control) cells, with DE defined as those with $q < 0.1$ calculated using the Storey method[63].

Bulk RNA-sequencing and analysis

CD4+ and CD8+ LTBR− or tNGFR-transduced T-cells were stimulated for 24 hours with CD3/CD28 Activator (25 μl per 10^6 cells) or left unstimulated ($n = 3$ biological replicates). Total RNA was extracted using the Direct-zol RNA purification kit (Zymo). The 3'-enriched RNA-sequencing library was prepared as described before[64]. In brief, RNA was reverse transcribed using SMARTScribe Reverse Transcriptase (Takara Bio) and a poly(dT) oligo containing a partial Nextera handle. Resulting cDNA was then PCR amplified for 3 cycles using OneTaq polymerase (NEB) and tagmented for 5 minutes at 55°C using homemade transposase TnY[65]. Immediately afterwards the tagmented DNA was purified on a MinElute column (Qiagen) and PCR amplified using OneTaq polymerase and barcoded primers for 12 cycles. The PCR product was purified using a dual (0.5X-0.8X) SPRI cleanup (Agencourt) and the size distribution was determined using Tapestation (Agilent). Samples were sequenced on a NextSeq 500 (Illumina) using a v2.5 75-cycle kit (paired end). Paired-end reads were aligned to the transcriptome (human Ensembl v96 reference[66]) using `kallisto` 0.46.0[55] and loaded into `RStudio` 1.1.419 with `R` 4.0.0.2

using `tximport` package[67]. Differential gene expression analysis was performed using `DESeq2`[50]. Gene ontology enrichment (biological process) on genes passing `DESeq2` criteria ($\log_2$[fold-change] > 1, $p_{adj.} < 0.05$) was performed using the topGO package[51].

ATAC-seq library preparation

CD8+ LTBR and tNGFR T-cells were stimulated for 24 hours with CD3/CD28 Activator (25 μl per 10^6 cells) or left unstimulated ($n = 2$ biological replicates). We performed bulk ATAC-seq as previously described[44]. Briefly, cell membranes were lysed in the RSB buffer (10mM Tris-HCL pH 7.4, 3mM $MgCl_2$, 10mM NaCl) with 0.1% IGEPAL freshly added. After pipetting up and down, nuclei were isolated by centrifugation at 500g for 5 minutes at 4°C. After discarding the supernatant, the nuclei were resuspended in the Tagmentation DNA (TD) Buffer[65] with homemade transposase TnY protein[65] and incubated at 37°C for 30 minutes. After purification on a MinElute column (Qiagen), the tagmented DNA was PCR amplified using a homemade Pfu X7 DNA polymerase[65] and barcoded primers for 12 cycles. The PCR product was purified via a 1.5X SPRI cleanup (Agencourt) and checked for a characteristic nucleosome banding pattern using TapeStation (Agilent). Samples were sequenced on a NextSeq 500 (Illumina) using the v2.5 75-cycle kit (single end).

ATAC-seq analysis

Single-end reads were aligned to the Gencode hg38 primary assembly[68] using `Bowtie2` v2.4.4[57]. We then used `Samtools` v1.9[69] to filter out alignments with low-mapping quality (MAPQ < 30) and subsequently to sort and index the filtered BAM files[69]. Read duplicates were removed using `Picard` v4.1.8.1[70]. Peaks were called using `MACS3` v3.0.0[71] with default parameters (`-g 2.7e9 -q 0.05`).

To construct the union feature space (“union peaks”) used for much of the downstream analyses, we began by performing intersections on pairs of biological replicate narrowPeak files using bedtools v2.29.0 (using `bedtools` intersect), keeping only those peaks found in both replicates[72]. After marking the shared peaks between replicates, we used `bedtools` merge to consolidate the biological replicates at each shared peak (at least 1 bp overlap). In this new peak BED file, each shared peak includes all sequence found under the peak in either of the biological replicates. Next, we took the union of each of these peak files (LTBR resting, LTBR stimulated, tNGFR resting, tNGFR stimulation); we combined any peaks with at least 1 base pair of overlap. Using the “union peaks”, we generated a peak read count matrix (union peaks x ATAC samples) where each entry in the matrix corresponds to the number of reads overlapping that peak in the specified sample — we term this the *per-peak* ATAC matrix. The overlapping reads are taken directly from the BAM files (converted to BED) that provide an alignment for each sample. Thus, the matrix includes a column for each biological replicate. Although samples had minimal differences in aligned reads, we normalised each entry in the matrix by the number of reads that overlapped the TSS regions in each sample. In this manner, any difference in read/alignment depth between samples would be normalized appropriately. In addition to the *per-peak* ATAC matrix, we also constructed a *per-gene* ATAC matrix as follows: We assigned a gene’s total ATAC reads as the sum of normalized reads from the *per-peak* ATAC matrix for all peaks within 3 kb of a gene’s start or end coordinates.

We imported these two ATAC matrices (*per-peak* and *per-gene*) into R v4.1.1 for gene and peak enrichment analysis using `DESeq2` v1.32.0. For comparison between ATAC-seq and RNA-seq, we used a statistical threshold of adjusted *p*-value < 0.05 and either $\log_2$(fold-change) > 0 (for increases in ATAC or RNA) or $\log_2$(fold-change) < 0 (for decreases in ATAC or RNA). For transcription factor-motif analysis we used `ChromVAR` v1.14.0[73] as follows: For each of the test vs. control conditions, we constructed `SummarizedExperiment` objects using column/sample subsets of the *per-peak* matrix and the union feature space. We used the `matchMotifs` function to annotate transcription factor-motifs. We computed enrichment deviations between test and control conditions using the `computeDeviations` function.

To produce read pileup tracks at specific genomic loci, we pooled de-duplicated reads from biological replicates (BAM) using `samtools` merge. We converted these pooled-replicate BAM files to bigWig files by using the `bamCoverage` function from `deeptools` v3.4.2 and setting the `scaleFactor` to the relative number of TSSs found in the pooled biological replicates compared to all other sample aggregates[74]. Using the bigWig files, read pileups were plotted with `pyGenomeTracks` v3.6[75].

Lastly, we performed *k*-means clustering on ATAC peaks near genes with increased chromatin accessibility. First, using DEseq2 on the ATAC *per-gene* matrix, we identified genes with $\log_2$(fold-change) > 1 and adjusted *p*-value < 0.05 (i.e. genes with increased chromatin accessibility) in either of two comparisons: 1) LTBR stimulated vs. tNGFR stimulated, 2) LTBR resting vs. tNGFR resting. After identifying these genes, we isolated all accessibility peaks in the *per-peak* ATAC matrix within 3kb of the gene body; this subset of peaks from the *per-peak* ATAC matrix was used as input for the clustering. Then, using `deeptools` (`computeMatrix` and `plotHeatmap` functions) on this subset of ATAC peaks, we performed *k*-means clustering with $k = 4$ clusters and 6 kb read windows.

Statistical analysis

Data between two groups were compared using a two-tailed unpaired Student's *t*-test or the Mann-Whitney test as appropriate for the type of data (depending on normality of the distribution). Unless otherwise indicated, a *P*-value less than or equal to 0.05 was considered statistically significant for all analyses, and not corrected for multiple comparisons. In cases where multiple comparison corrections were necessary, we adjusted the *P*-value using the Benjamini-Hochberg method. All group results are represented as mean ± s.e.m, if not stated otherwise. Statistical analyses were performed in Prism (GraphPad) and RStudio (Rstudio PBC). Flow cytometry data was analysed using FlowJo 10.7.1 (Treestar).

Extended Data

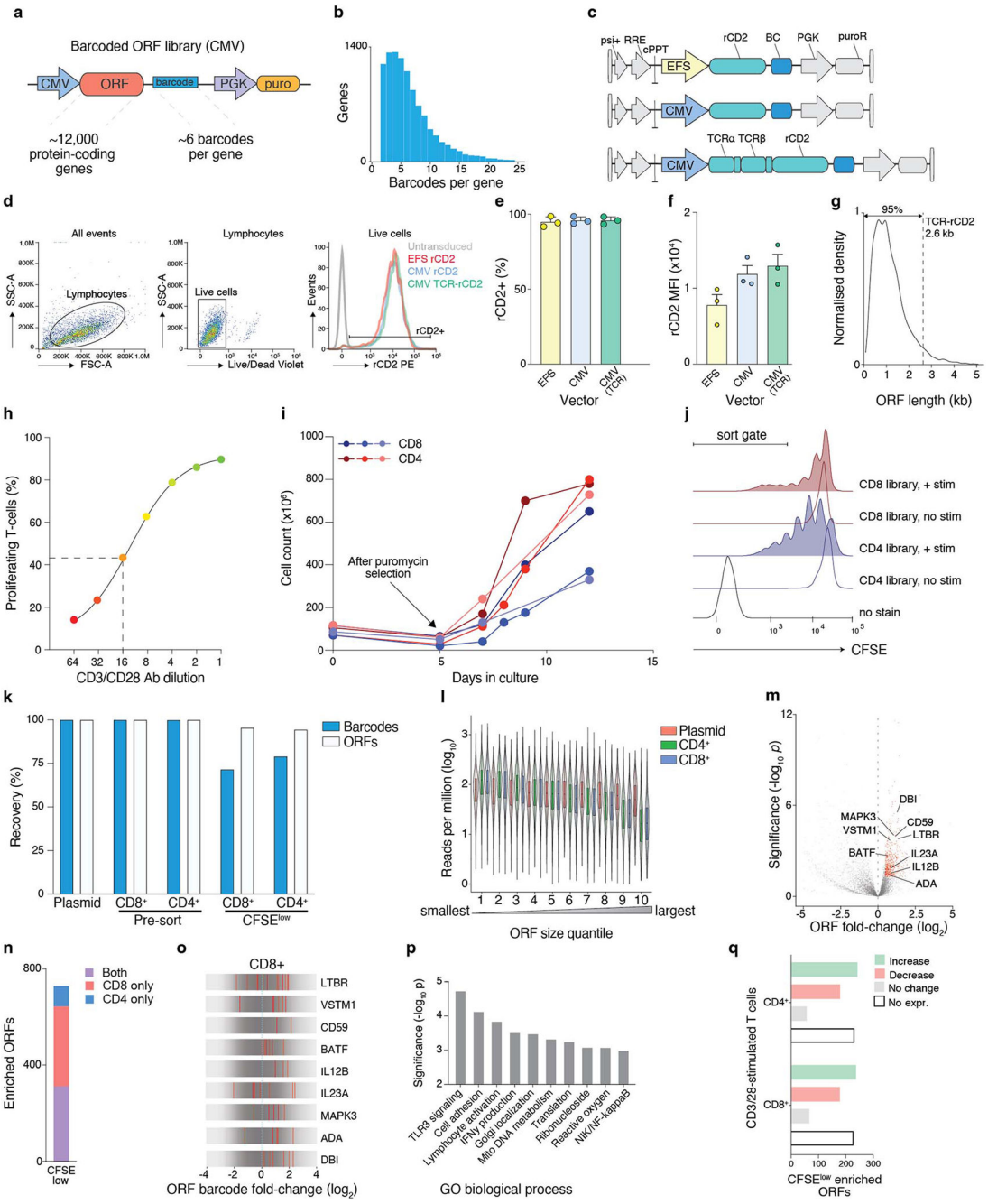

Extended Data Figure 1. Design of human ORF library screen in primary T-cells.

a) Barcoded vector design for ORF overexpression. **b**) Distribution of the number of barcodes per ORF in the library. **c**) Vector design for quantifying the effect of different promoters and ORF insert sizes on lentiviral transduction efficiency. EFS – elongation factor-1α short promoter, CMV – cytomegalovirus promoter, PGK – phosphoglycerate kinase-1 promoter. **d**) Sequential gating strategy and representative histograms of cells transduced with marker gene rat CD2 under different promoters. **e**) Percentage of positive

cells and (**f**) mean fluorescence intensity (MFI) of rat CD2 (rCD2) expressed from the EFS and CMV promoters, following puromycin selection of transduced primary CD4+ T-cells. Each data point indicates individual transduction (n = 3 biological replicates). Error bars are SEM. **g**) Distribution of ORF sizes in the genome-scale library. The size of TCR-rCD2 construct tested in panels *e* and *f* is marked. **h**) Titration of CD3/CD28 antibodies. T-cells were labelled with CFSE, stimulated and incubated for 4 days. Gate for proliferating T-cells was set to include cells that proliferated at least twice (third CFSE peak). **i**) Expansion of T cells from three healthy donors transduced with the ORF library. **j**) Representative CFSE profile of restimulated CD8+ and CD4+ T cells before the sort. The $CFSE^{low}$ sort gate is marked. **k**) Recovery of individual barcodes or corresponding ORFs in transduced T cells and plasmid used for lentivirus production. Respective samples from three donors were computationally pooled together at equal number of reads prior to counting how many barcodes or ORFs were present with a minimum of one read. **l**) Distribution of reads corresponding to ORFs of different sizes. ORFs were assigned to ten quantiles based on their size, with Q1 being smallest size and Q10 being the largest size (n = 1,161 ORFs per quantile). Box shows 25-75 percentile with a line at the median while whiskers extend to 1.5x interquartile range. **m**) Enrichment of genes in both $CFSE^{low}$ CD4+ and CD8+ T-cells, calculated by collapsing individual barcodes into corresponding genes. Significantly-enriched genes ($\log_2$ fold change higher than 0.5 and adjusted p-value lower than 0.05) are marked in red. Immune response genes of interest are marked. **n**) Overlap of significantly-enriched genes from panel *m* in individual screen populations (CD4+, CD8+) analysed separately. **o**) Normalised enrichment of individual barcodes for indicated genes in the CD8+ screen. **p**) GO biological processes for significantly-enriched genes in panel *m*. (**q**) Overlap of significantly-enriched genes with differentially-expressed genes between CD3/CD28 stimulated and naïve T-cells[41].

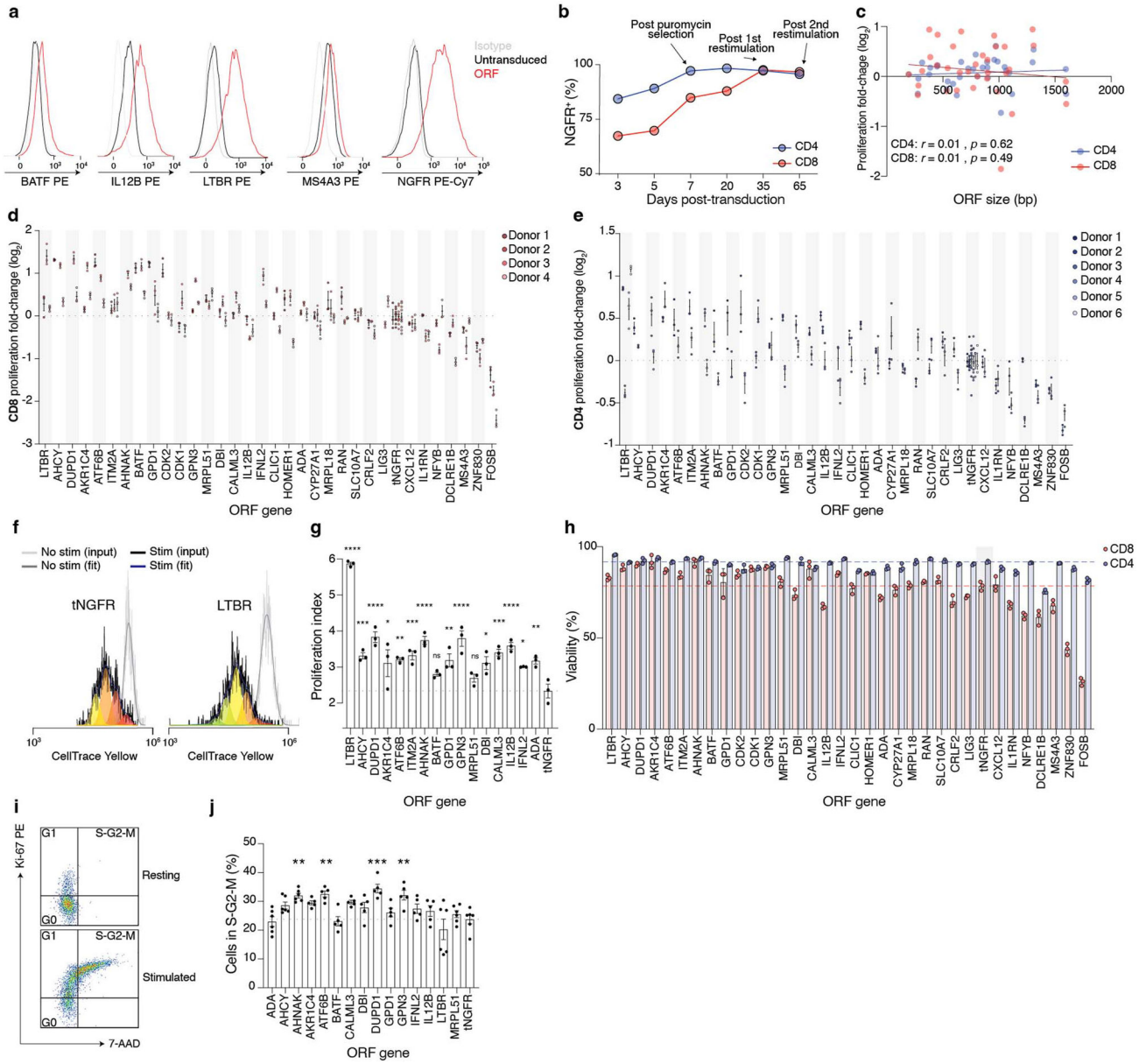

Extended Data Figure 2. Overexpression of select ORFs in screen-independent donors.

a) Histograms of selected ORF expression in T cells after puromycin selection. **b**) Quantification of tNGFR expression in transduced CD4+ and CD8+ T cells. Puromycin selection was complete after 7 days post transduction. To maintain T cells in culture, they were re-stimulated with CD3/CD28 on days 21 and 42. **c**) Correlation between ORF sizes and changes in proliferation relative to tNGFR. Mean $\log_2$ fold-changes are shown. **d**) Proliferation of restimulated CD8+ or **e**) CD4+ T cells relative to tNGFR in individual donors (n = 3 biological replicates). Mean and SEM are shown. **f, g**) Proliferation of T-cells transduced with ORFs that significantly improved T-cell proliferation (see Fig. 2c) measured by dilution of CellTrace Yellow. Representative CellTrace Yellow histograms and fitted distributions (*f*) as well as quantifications of the proliferation index (*g*) are shown (n = 3 biological replicates). P values: <0.0001, 0.0008, <0.0001, 0.011, 0.0031, 0.0007,

<0.0001, 0.28, 0.004, <0.0001, 0.58, 0.01, 0.0003, <0.0001, 0.036, 0.0049 (left to right). **h**) Viability of ORF-transduced T-cells 4 days after CD3/CD28 restimulation. Representative data from one donor (out of 4 donors tested) are shown (n = 3 biological replicates), **i, j**) Cell cycle analysis of T-cells stimulated with CD3/CD28 for 24 h. Gating was performed based on isotype and fluorescence minus one controls. Representative gating (i) as well as (j) quantification of cells in the S-G2-M phases (for stimulated T-cells) are shown (n = 6 biological replicates from two donors). P values: 1, 0.29, 0.0065, 0.17, 0.0051, 1, 0.13, 0.55, 0.0004, 0.98, 0.0088, 0.68, 0.91, 0.7, 1 (left to right).

Statistical significance for panels g and j: one way ANOVA with Dunnett's multiple comparisons test * p<0.05, ** p<0.01, *** p<0.001, **** p<0.0001. Error bars indicate SEM.

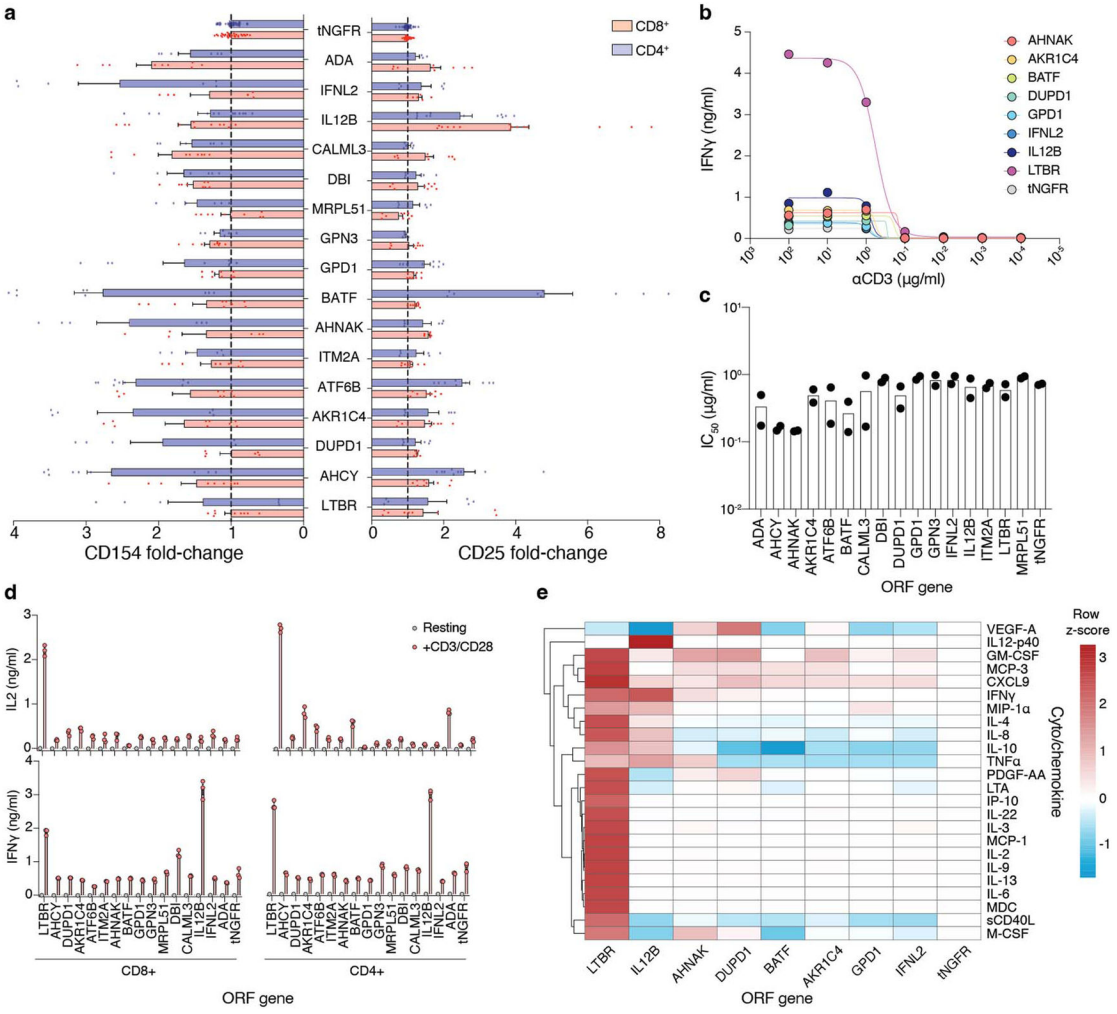

Extended Data Figure 3. Functional response of ORF-overexpressing T-cells.

a) Quantitative expression of CD25 or CD154 following re-stimulation. A minimum of two donors was tested in triplicate per gene. Only genes that significant increase T-cell proliferation in CD4+, CD8+ or both T-cell subsets are shown. Mean and SEM are shown. **b,c**) Sensitivity to antigen dose. T-cells were incubated with indicated anti-CD3 antibody

concentrations for 24 h and the amount of secreted IFNγ was quantified. Representative dose-response curve fitting (*b*) and IC50 quantifications (*c*) are shown ($n = 2$ biological replicates). **d**) Quantification of secreted IL-2 and IFNγ in T-cells incubated alone or with CD3/CD28 antibodies for 24 h. Representative data from one out of four donors ($n = 3$ biological replicates) are shown. **e**) Multiplexed quantification of selected secreted cytokines and chemokines by ORF-transduced T cells after 24 h of CD3/CD28 stimulation. Means of duplicate measurements (from independent samples) *z*-score normalised to tNGFR are shown. Absolute quantities of secreted cytokines and chemokines in stimulated and resting T cells are shown in Supplementary Table 7.

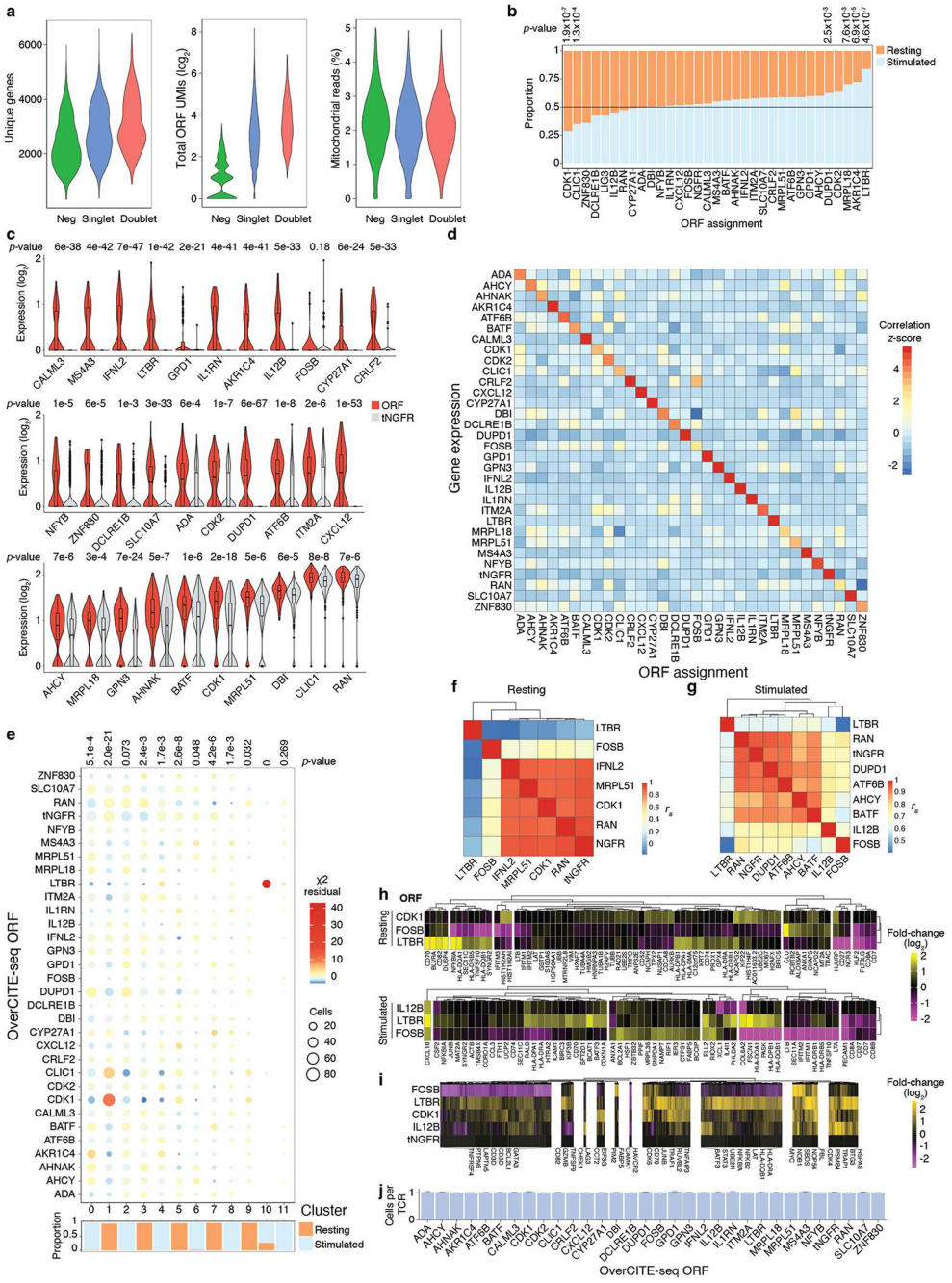

Extended Data Figure 4. OverCITE-seq identifies ORFs and their transcriptional effects.

a) Quality parameters of cells as identified by gel bead barcodes. Negative, singlets and doublets are assigned based on cell hashing. **b**) Proportion of stimulated and resting T-cells among cells assigned to each ORF. Chi-squared test *p*-values are shown for ORFs with significantly shifted (uneven) distributions of stimulated and rested cells. **c**) Cell-cycle corrected scaled expression of the overexpressed gene in the cells transduced with the respective ORF and negative control (tNGFR). Two-sided Wilcoxon test *p*-values shown above the violin plots indicate the statistical significance of gene expression level between specific ORF and tNGFR-transduced T-cells. Box shows 25-75 percentile with a line at

the median while whiskers extend to maximum and minimum values. $N = 71$ (ADA), 147 (AHCY), 190 (AHNAK), 119 (AKR1C4), 124 (ATF6B), 179 (BATF), 137 (CALML3), 189 (CDK1), 129 (CDK2), 236 (CLIC1), 84 (CRLF2), 91 (CXCL12), 88 (CYP27A1), 129 (DBI), 26 (DCLRE1B), 261 (DUPD1), 25 (FOSB), 119 (GPD1), 124 (GPN3), 199 (IFNL2), 60 (IL12B), 70 (IL1RN), 156 (ITM2A), 74 (LTBR), 88 (MRPL18), 167 (MRPL51), 107 (MS4A3), 69 (NFYB), 355 (NGFR), 261 (RAN), 182 (SLC10A7), and 56 (ZNF830) single cells. **d**) Expression of all ORF genes by cells assigned each ORF. Each row is z-score normalised. **e**) Distribution of individual ORF frequencies in clusters. Numbers of ORF cells and the chi-squared test residuals are displayed. Chi-squared test *p*-values indicating whether ORF distribution in each cluster significantly differs from overall ORF distribution are shown on top of the plot. Proportions of stimulated and resting T-cells in each cluster are shown underneath the cluster label. **f,g**) Spearman correlations between transcriptional profiles of selected ORF cells in resting (*f*) and stimulated (*g*) populations. **h**) Fold change of top differentially expressed genes between cells with the indicated ORFs in resting and stimulated T-cells. For each condition, the ORFs with the strongest transcriptional changes (compared to tNGFR cells) are shown. **i**) Differential gene expression in stimulated ORF T-cells compared to resting T-cells. Genes with significant expression changes in at least one ORF are shown (DESeq2 adjusted $p < 0.05$). For all genes, we display $\log_2$ fold-change of each ORF (stimulated) to tNGFR (resting), normalised to $\log_2$ fold-change of tNGFR (stimulated) to tNGFR (resting). Genes of interest in each cluster are labelled. **j**) Mean TCR clonotype diversity in ORF cells.

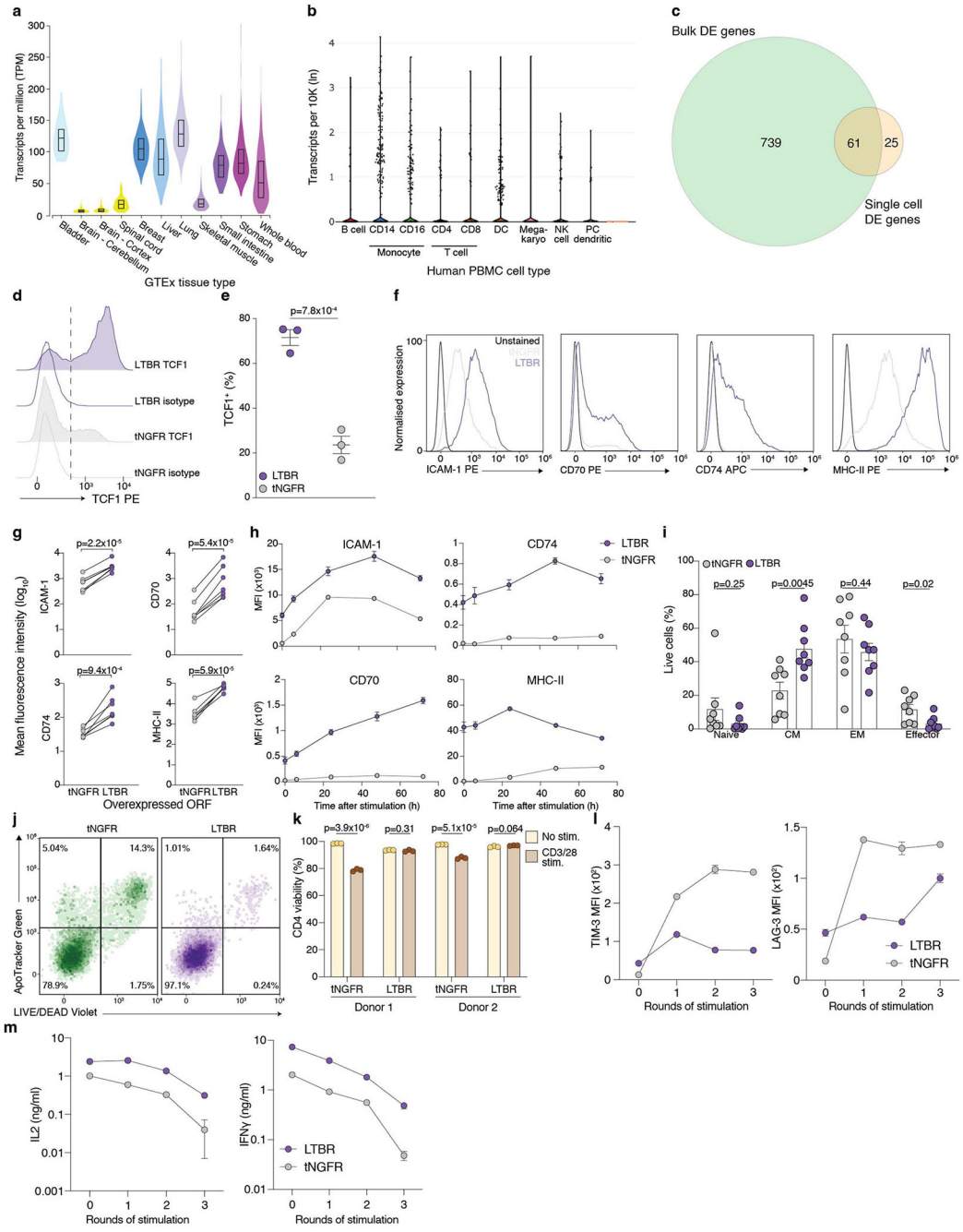

Extended Data Figure 5. Functional analysis of LTBR overexpression in T-cells.

a) *LTBR* expression in the indicated human primary tissues from the Genotype-Tissue Expression (GTEx) project v8[76] (n = 948 donors). Box shows 25-75 percentile with a line at the median. **b**) *LTBR* expression in peripheral blood mononuclear cells (PBMCs) from 31,021 cells from 2 donors[77]. Cell types indicated are derived from Harmony tSNE clustering of single-cell transcriptomes. **c**) Overlap between significantly upregulated genes in LTBR cells compared to tNGFR cells identified in single-cell or bulk RNA-seq. **d,e**) TCF1 expression in LTBR or tNGFR transduced T-cells. *d*) Representative histograms of TCF1 expression and the gate for TCF1+ cells (dashed line) are shown, as well as

(*e*) quantification of TCF1+ cells ($n = 3$ biological replicates). **f-h**) ICAM-1, CD70, CD74, and MHC-II expression in LTBR and tNGFR T-cells. Representative histograms (*f*), quantification (*g*) in $n = 3$ donors (CD8+) or $n = 4$ donors (CD4+) and timecourse (*h*) of expression in LTBR and tNGFR cells after CD3/CD28 stimulation ($n = 3$ biological replicates). **i**) Differentiation phenotype of NGFR and LTBR transduced T cells ($n =$ 4 donors, CD4+ and CD8+ separately). CM: Central memory. EM: Effector memory. Differentiation was defined based on CD45RO and CCR7 expression (naïve: $CD45RO^{neg}$ $CCR7^{+}$, CM: $CD45RO^{+}$ $CCR7^{+}$, EM: $CD45RO^{+}$ $CCR7^{neg}$, effector $CD45RO^{neg}$ $CCR7^{neg}$). **j**) Representative dot plots of T-cell viability after CD3/CD28 stimulation. Viable cells are in the lower left quadrant. **k**) Cell viability of CD4+ T-cells transduced with LTBR or tNGFR lentivirus, either re-stimulated with CD3/CD28 for four days or left unstimulated ($n = 2$ donors with 3 biological replicates each). **l,m**) LTBR and tNGFR cells were stimulated with a 3:1 excess of CD3/CD28 beads every three days for up to three rounds of stimulation. Following repeated stimulation, expression of TIM-3 and LAG-3 (*l*) was measured in resting cells, and secretion of IFNγ and IL2 (*m*) was measured in restimulated cells (n = 3 biological replicates).

Statistical significance for panels *e, i,* and *k:* two-sided unpaired *t*-test; for panel *g*: two-sided paired *t*-test. Error bars indicate SEM.

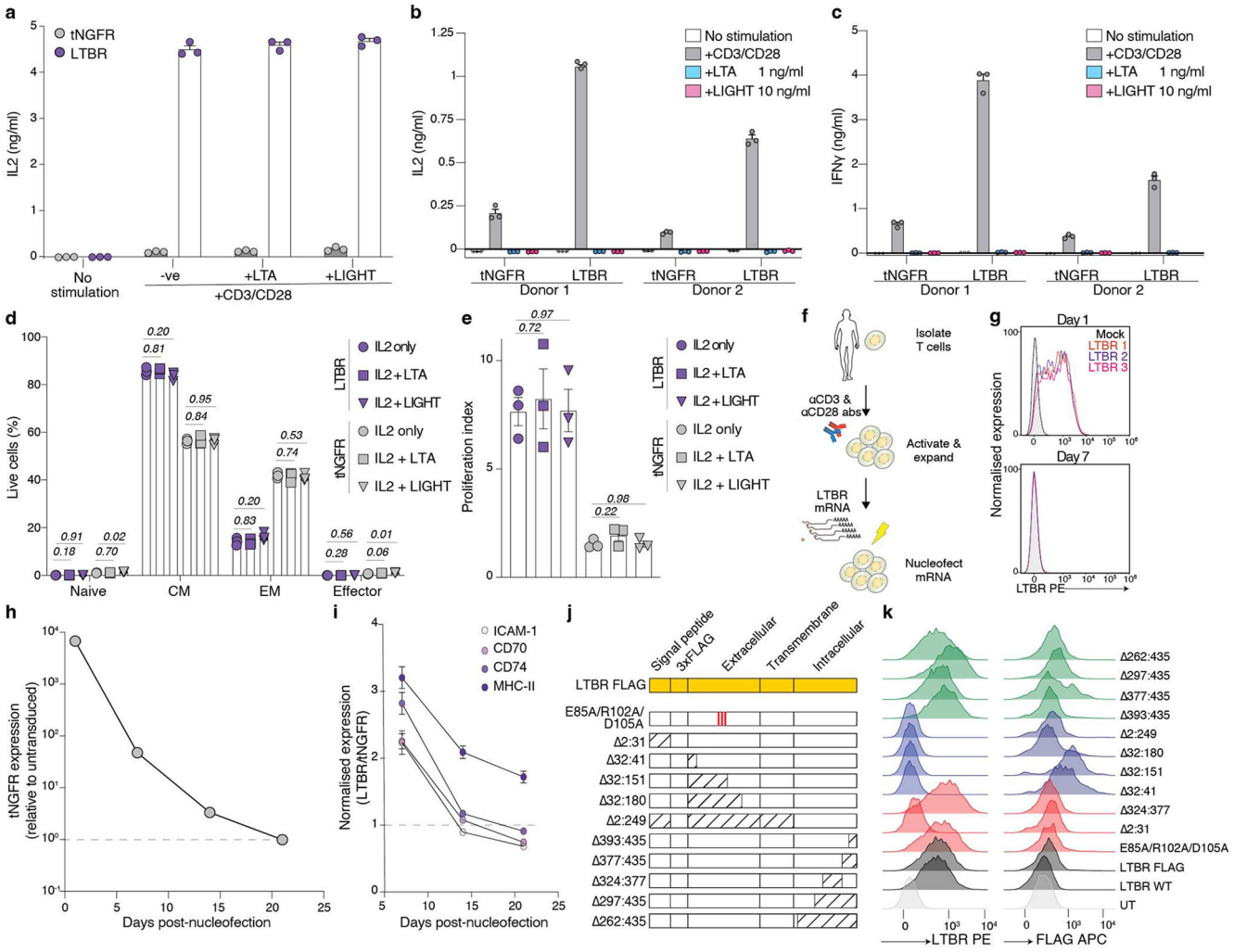

Extended Data Figure 6. LTBR ligands and expression of LTBR via mRNA or with deletion and point mutants.

a) IL2 secretion after 24 hour stimulation with CD3/CD28 antibodies. Where indicated, recombinant soluble LTA (1 ng/mL) or LIGHT (10 ng/mL) were added together with CD3/CD28 antibodies. CD4+ T cells from one donor were tested in triplicate. **b,c**) CD4+ and CD8+ T cells from two donors were co-incubated for 24 hours with CD3/CD28 antibodies or recombinant soluble LTA or LIGHT and then IL2 (*b*) and IFNγ (*c*) were measured. ($n = 3$ biological replicates). **d,e**) Differentiation phenotype (*d*) or proliferation (*e*) after restimulation of tNGFR and LTBR transduced T cells ($n = 3$ biological replicates) incubated either with IL2 alone or with LTA (1 ng/mL) or LIGHT (10 ng/mL) for the duration of culture. CM: Central memory. EM: Effector memory. Unpaired two-sided *t*-test *p* values are shown. **f-i**) Transient LTBR or tNGFR expression via mRNA nucleofection (*f*). T-cells were either nucleofected with LTBR or tNGFR mRNA ($n = 3$ biological replicates), and the surface expression of LTBR (*g*), tNGFR (*h*) or four genes upregulated in LTBR cells (*i*) was monitored over 21 days. At each timepoint the expression of target genes was normalised to matched tNGFR control. **j**) Schematic representation of FLAG-tagged LTBR mutants. **k**) LTBR and FLAG expression in T-cells transduced with LTBR mutants.

Error bars indicate SEM.

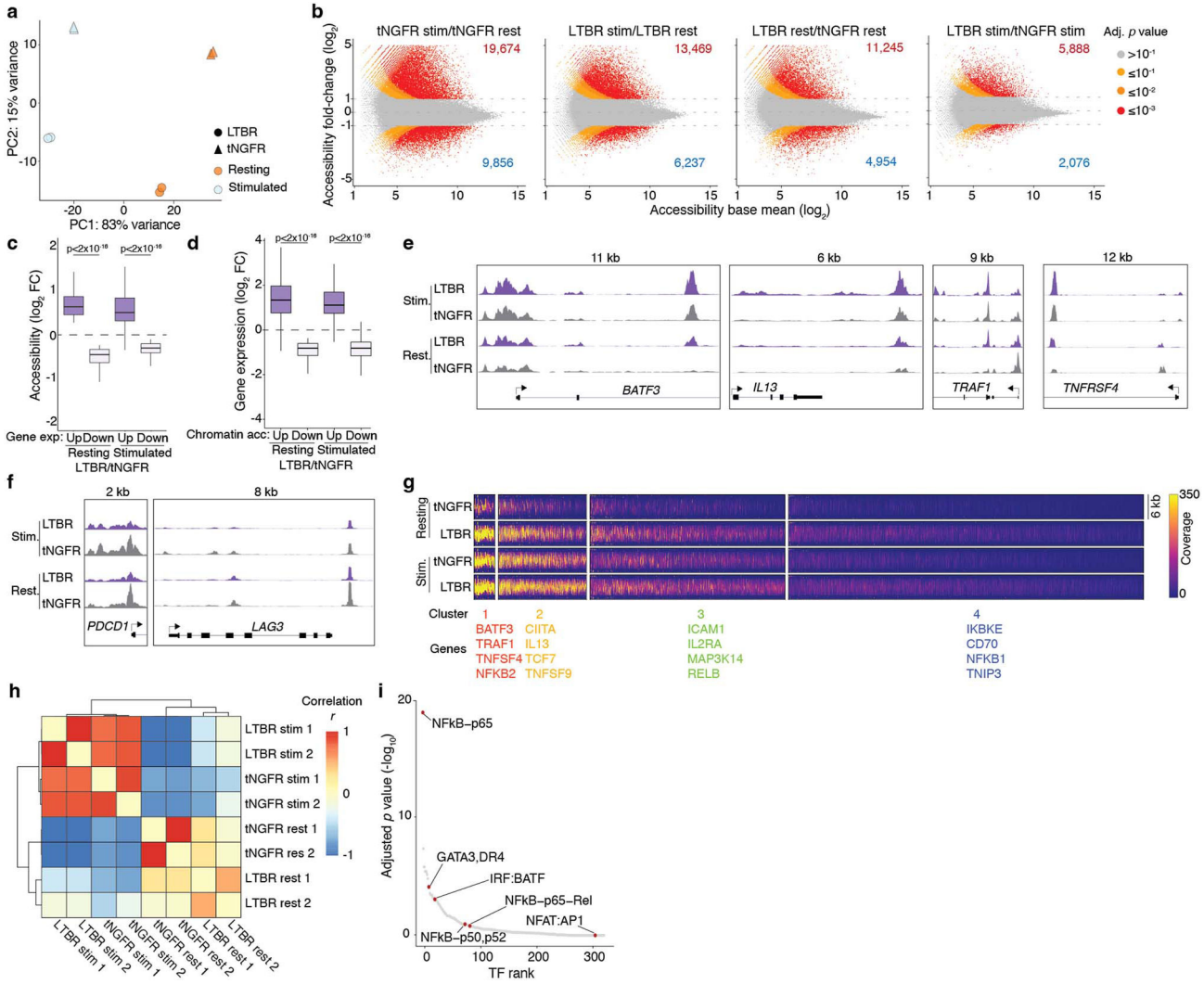

Extended Data Figure 7. Chromatin accessibility in LTBR T-cells.

a) Principal component (PC) analysis of global accessible chromatin regions of LTBR and tNGFR T-cells, either resting or stimulated with CD3/CD28 for 24 hours. **b**) Differentially accessible chromatin regions between stimulated and resting tNGFR, stimulated and resting LTBR, resting LTBR and resting tNGFR, and stimulated LTBR and stimulated tNGFR. Numbers of peaks gained/lost are shown (using absolute $\log_2$ fold change of 1 and adjusted *p* value < 0.1 as cut-off). **c, d**) Changes in chromatin accessibility (*c*) for differentially expressed (adjusted $p<0.05$) genes or in gene expression (*d*) for differentially accessible (adjusted $p<0.05$) regions. Two-sided *t*-test *p* values are shown. Box shows 25-75 percentile with a line at the median while whiskers extend to 1.5x interquartile range. $N = 614$ genes (*c*) or genomic regions (*d*). **e, f**) Chromatin accessibility profiles at loci more (*e*) or less open (*f*) in LTBR compared to tNGFR cells, resting or stimulated for 24 hours. The *y*-axis represents normalised reads (scale: 0-860 for *BATF3*, 0-1950 for *IL13*, 0-1230 for *TRAF1*, 0-1000 for *TNFSF4*, 0-300 for *PDCD1*, 0-2350 for *LAG3*). **g**) Chromatin accessibility in

resting or stimulated LTBR and tNGFR cells. Each row represents a peak significantly enriched in LTBR over matched tNGFR control (log_2 fold change > 1, DESeq2 adjusted *p* value < 0.05). Peaks were clustered using *k*-means clustering and selected genes at/near peaks from each cluster are indicated. **h**) Correlations for each ATAC sample (biological replicate) based on the bias-corrected deviations. **i**) Top transcription factor (TF) motifs enriched in the differentially accessible chromatin regions in resting LTBR cells compared to resting tNGFR cells.

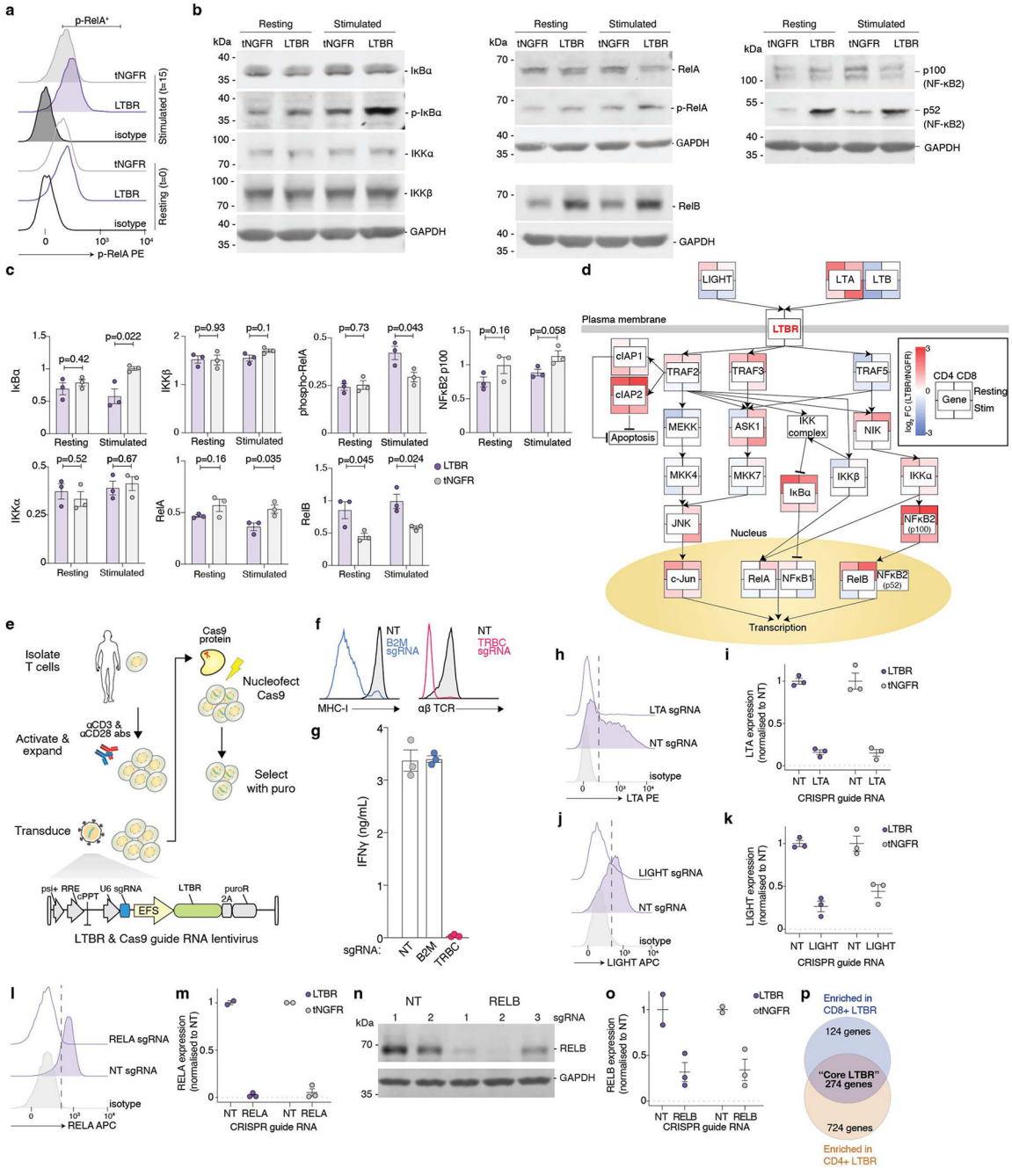

Extended Data Figure 8. Proteomic and functional genomic assays of NF-κB activation.

a) Phospho-RelA staining by intracellular flow cytometry in LTBR and tNGFR cells. Gating for identification of phospho-RelA+ cells is shown. **b, c)** Western blot quantification of key proteins in the NF-κB pathway in LTBR and tNGFR cells, resting or stimulated with CD3/CD28 for 15 min. Representative gels (*b*) or quantification of band intensity relative to GAPHD (*c*) are shown ($n = 3$ biological replicates). Unpaired two-sided *t* test *p* values are shown. **d**) Representation of the LTBR signalling pathway. Each gene is coloured based on the differential expression in LTBR over matched tNGFR cells (CD4+ and CD8+ T-cells, resting or stimulated for 24 hours). **e-g**) Simultaneous gene knockout via CRISPR and ORF overexpression. T-cells were transduced with a lentiviral vector co-expressing a single guide RNA (sgRNA) and the LTBR ORF. After transduction, Cas9 protein was delivered via nucleofection. **f**) Representative expression of target genes in LTBR cells co-expressing an sgRNA targeting *B2M*, an essential component of the MHC-I complex, or *TRBC1/2*, an essential component of the αβ TCR. **g**) Quantification of IFNγ after restimulation ($n = 3$ sgRNAs). **h-o**) Representative protein-level based quantification of gene knockout efficiency. Representative histograms (*h, j, l*) and quantification of relative expression levels of LTA, LIGHT, and RELA (*i, k, m*) are shown ($n = 3$ sgRNAs). Dashed lines represent gates used to enumerate cells expressing a given protein. Representative gel (*n*) and quantification of RELB expression (*o*) are shown ($n = 3$ sgRNAs for RELB and 2 non-targeting control sgRNAs). **p**) Identification of 274 genes identified as enriched in both CD4+ and CD8+ T-cells transduced with LTBR over matched tNGFR controls (“core LTBR” genes).

See Supplementary Figure 1 for uncropped gel images. Error bars indicate SEM.

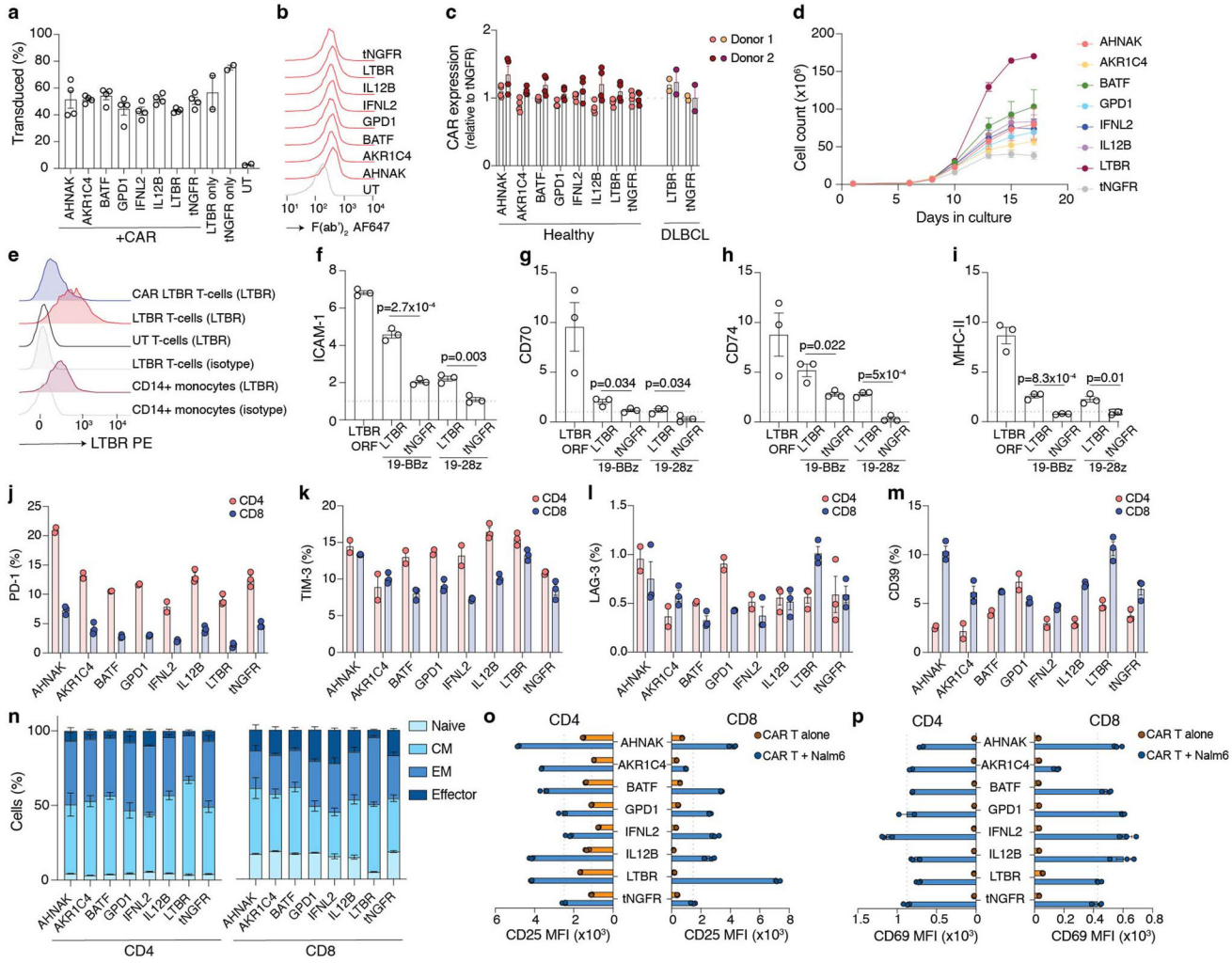

Extended Data Figure 9. Co-delivery of ORFs with CD19-targeting CARs.

a) Transduction efficiency of CAR+ORF lentiviral vectors or ORF alone (*n* = 4 biological replicates). **b,c**) CAR expression level as determined by staining with anti-mouse Fab F(ab')$_2$-Representative histograms (*b*) and quantification of CAR expression relative to tNGFR (*c*) is shown for two healthy donors and two diffuse large B-cell lymphoma (DLBCL) patients, **d**) Expansion curves of CAR+ORF transduced T-cells (*n* = 4 biological replicates). **e**) LTBR expression in autologous CD14+ monocytes and T-cells transduced with LTBR alone or CAR+LTBR. **f-i**) Expression of ICAM-1 (*f*), CD70 (*g*), CD74 (*h*) and MHC-II (*i*) by T-cells transduced with LTBR ORF only, CAR+LTBR or CAR+tNGFR. All data are normalised to tNGFR only (no CAR). Unpaired two-sided *t* test *p* values are shown. **j-m**) Expression of exhaustion markers PD-1 (*j*), TIM-3 (*k*), LAG-3 (*l*) and CD39 (*m*) in CAR+ORF T-cells. **n**) Differentiation phenotype of CAR+ORF T-cells. CM: Central memory. EM: Effector memory. Differentiation was defined based on CD45RO and CCR7 expression (naïve: CD45RO^{neg} CCR7^{+}, CM: CD45RO^{+} CCR7^{+}, EM: CD45RO^{+} CCR7^{neg}, effector CD45RO^{neg} CCR7^{neg}). **o,p**) Expression of activation markers CD25 (*o*) and CD69 (*p*) in CAR+ORF T-cells incubated alone or with Nalm6 cells for 24 hours. Error bars indicate SEM. *N* = 3 biological replicates, unless indicated otherwise.

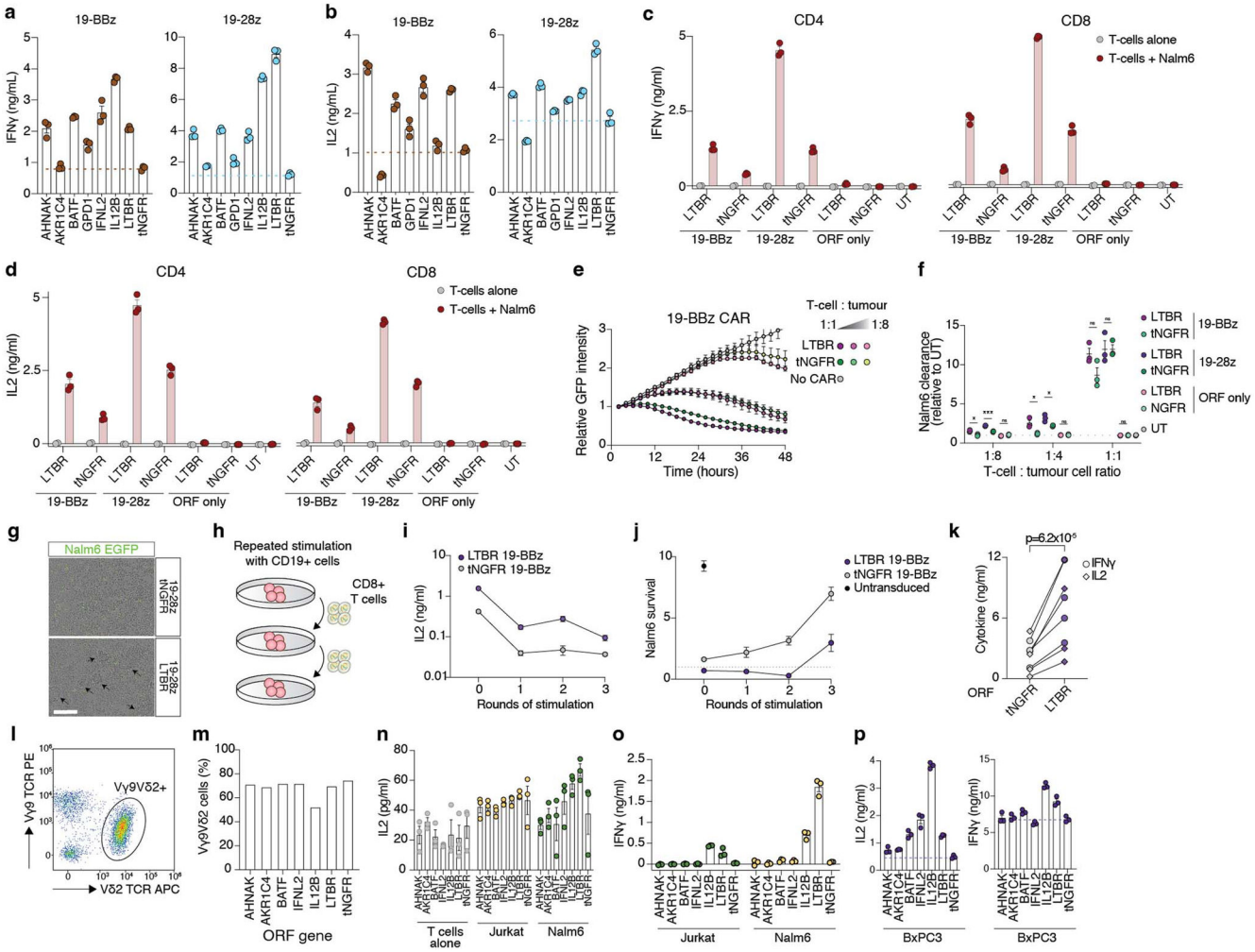

Extended Data Figure 10. Top-ranked genes from the ORF screen boost antigen-specific T cell responses.

a,b) Co-delivery of anti-CD19 CARs and ORFs to T-cells from healthy donors. (*a*) IFNγ and (*b*) IL2 secretion after overnight co-incubation of CD4+ T-cells with Nalm6 cells at 1:1 ratio ($n = 3$ biological replicates, representative of two donors). **c,d**) IFNγ (*c*) or IL-2 (*d*) secretion by CAR+ORF or ORF only T-cells co-incubated for 24 hours either alone or with Nalm6 cells. **e**) Cytotoxicity of 19-BBz CAR T cells expressing tNGFR or LTBR ORF after co-incubation with Nalm6 GFP cells. **f**) Quantification of Nalm6 clearance (relative to Nalm6 co-incubated with untransduced T-cells) for CAR+ORF or ORF alone T-cells at different effector:target ratios. Unpaired two-sided *t*-test *p* values: 0.011, $1.3\text{x}10^{-4}$, 0.072, 0.02, 0.021, 0.52, 0.087, 1, 0.51 (left to right). **g**) Representative images of T cells transduced with 19-28z CAR and NGFR or LTBR, co-incubated with CD19+ Nalm6 GFP cells for 48 hours at 1:1 ratio. Scale bar: 200 μm. **h-j**) Repeated stimulation of CAR+ORF T-cells with Nalm6 cells. IL-2 secretion (*i*), or Nalm6 survival (*j*), by 19-BBz CAR LTBR or tNGFR T-cells re-challenged with Nalm6 after repeated stimulation with Nalm6 cells every three days, for up to three rounds of stimulation. **k**) Secretion of cytokines IL2 and IFNγ by CAR/LTBR or CAR/tNGFR T-cells from two DLBCL patients after overnight incubation

with Nalm6 target cells. Two-sided paired *t*-test *p* value is shown. **l**) Representative staining of ORF-transduced T cells endogenously expressing Vγ9Vδ2 TCR. **m**) Quantification of ORF-transduced T cells expressing Vγ9Vδ2 TCR. **n,o**) IL2 (*n*) or IFNγ (*o*) secretion after 24 hours co-incubation of ORF transduced Vγ9Vδ2 T cells with leukaemia cell lines. **p**) IL2 or IFNγ secretion after 24 hours co-incubation of ORF transduced Vγ9Vδ2 T cells with BxPC3, a pancreatic ductal adenocarcinoma cell line. Cell lines in panels *n-p* were pre-treated with zoledronic acid prior to co-incubation.

Error bars indicate SEM. $N = 3$ biological replicates are shown, unless indicated otherwise.

Extended Data References

76. GTEx Consortium. The GTEx Consortium atlas of genetic regulatory effects across human tissues. Science 369, 1318–1330 (2020). [PubMed: 32913098]
77. Ding J et al. Systematic comparative analysis of single cell RNA-sequencing methods. http://biorxiv.org/lookup/doi/10.1101/632216 (2019) doi:10.1101/632216.

Supplementary Material

Refer to Web version on PubMed Central for supplementary material.

Acknowledgements

We thank the entire Sanjana laboratory for support and advice. We thank the NYU Biology Genomics Core for sequencing resources. M.L. is supported by the Hope Funds for Cancer Research postdoctoral fellowship. Z.G. is supported by the National Institutes of Health (NIH) T32 Training Grant (GM136573). N.E.S. is supported by NYU and NYGC startup funds, NIH/NHGRI (nos. R00HG008171 and DP2HG010099), NIH/NCI (no. R01CA218668), DARPA (no. D18AP00053), Cancer Research Institute, and the Sidney Kimmel Foundation.

Data availability

Data from the ORF screen, OverCITE-seq, bulk RNA-seq, and ATAC-seq have been deposited in GEO (accession number: GSE193736). The following publicly available datasets have also been used in the study: Database of Immune Cell eQTLs, Expression, Epigenomics (https://dice-database.org/), Genotype-Tissue Expression Project v8 (https://www.gtexportal.org/), and Single Cell Portal (https://singlecell.broadinstitute.org/single_cell/study/SCP424/single-cell-comparison-pbmc-data).

References

1. Abramson JS et al. Transcend NHL 001: Immunotherapy with the CD19-Directed CAR T-Cell Product JCAR017 Results in High Complete Response Rates in Relapsed or Refractory B-Cell Non-Hodgkin Lymphoma. Blood 128, 4192–4192 (2016).
2. Shifrut E et al. Genome-wide CRISPR Screens in Primary Human T Cells Reveal Key Regulators of Immune Function. Cell 175, 1958–1971.e15 (2018). [PubMed: 30449619]
3. Dong MB et al. Systematic Immunotherapy Target Discovery Using Genome-Scale In Vivo CRISPR Screens in CD8 T Cells. Cell 178, 1189–1204.e23 (2019). [PubMed: 31442407]
4. Chen Z et al. In vivo CD8+ T cell CRISPR screening reveals control by Fli1 in infection and cancer. Cell 184, 1262–1280.e22 (2021). [PubMed: 33636129]
5. Kabelitz D, Serrano R, Kouakanou L, Peters C & Kalyan S Cancer immunotherapy with γδ T cells: many paths ahead of us. Cell Mol Immunol 17, 925–939 (2020). [PubMed: 32699351]
6. Munshi NC et al. Idecabtagene Vicleucel in Relapsed and Refractory Multiple Myeloma. New England Journal of Medicine 384, 705–716 (2021). [PubMed: 33626253]

7. Fraietta JA et al. Determinants of response and resistance to CD19 chimeric antigen receptor (CAR) T cell therapy of chronic lymphocytic leukemia. Nat Med 24, 563–571 (2018). [PubMed: 29713085]
8. Singer M et al. A Distinct Gene Module for Dysfunction Uncoupled from Activation in Tumor-Infiltrating T Cells. Cell 166, 1500–1511.e9 (2016). [PubMed: 27610572]
9. Gurusamy D et al. Multi-phenotype CRISPR-Cas9 Screen Identifies p38 Kinase as a Target for Adoptive Immunotherapies. Cancer Cell 37, 818–833.e9 (2020). [PubMed: 32516591]
10. Legut M, Dolton G, Mian AA, Ottmann OG & Sewell AK CRISPR-mediated TCR replacement generates superior anticancer transgenic T cells. Blood 131, 311–322 (2018). [PubMed: 29122757]
11. Ren J et al. Multiplex Genome Editing to Generate Universal CAR T Cells Resistant to PD1 Inhibition. Clin Cancer Res 23, 2255–2266 (2017). [PubMed: 27815355]
12. Wagner DL et al. High prevalence of Streptococcus pyogenes Cas9-reactive T cells within the adult human population. Nat Med 25, 242–248 (2019). [PubMed: 30374197]
13. Wu X et al. Genome-wide binding of the CRISPR endonuclease Cas9 in mammalian cells. Nature Biotechnology 32, 670–676 (2014).
14. Sack LM et al. Profound Tissue Specificity in Proliferation Control Underlies Cancer Drivers and Aneuploidy Patterns. Cell 173, 499–514.e23 (2018). [PubMed: 29576454]
15. Yuan J et al. CTLA-4 blockade enhances polyfunctional NY-ESO-1 specific T cell responses in metastatic melanoma patients with clinical benefit. Proceedings of the National Academy of Sciences 105, 20410–20415 (2008).
16. Sommermeyer D et al. Chimeric antigen receptor-modified T cells derived from defined CD8+ and CD4+ subsets confer superior antitumor reactivity in vivo. Leukemia 30, 492–500 (2016). [PubMed: 26369987]
17. Fischer AM, Katayama CD, Pagès G, Pouysségur J & Hedrick SM The Role of Erk1 and Erk2 in Multiple Stages of T Cell Development. Immunity 23, 431–443 (2005). [PubMed: 16226508]
18. Lipp AM et al. Lck Mediates Signal Transmission from CD59 to the TCR/CD3 Pathway in Jurkat T Cells. PLoS ONE 9, e85934 (2014). [PubMed: 24454946]
19. Ma X et al. Interleukin-23 engineering improves CAR T cell function in solid tumors. Nat Biotechnol 38, 448–459 (2020). [PubMed: 32015548]
20. Seo H et al. BATF and IRF4 cooperate to counter exhaustion in tumor-infiltrating CAR T cells. Nat Immunol 22, 983–995 (2021). [PubMed: 34282330]
21. Jamali A et al. Highly Efficient and Selective CAR-Gene Transfer Using CD4− and CD8-Targeted Lentiviral Vectors. Molecular Therapy - Methods & Clinical Development 13, 371–379 (2019). [PubMed: 30997367]
22. Stoeckius M et al. Simultaneous epitope and transcriptome measurement in single cells. Nature Methods 14, 865–868 (2017). [PubMed: 28759029]
23. Mimitou EP et al. Multiplexed detection of proteins, transcriptomes, clonotypes and CRISPR perturbations in single cells. Nature Methods 16, 409–412 (2019). [PubMed: 31011186]
24. Gil-Yarom N et al. CD74 is a novel transcription regulator. Proc Natl Acad Sci USA 114, 562–567 (2017). [PubMed: 28031488]
25. Ataide MA et al. BATF3 programs CD8+ T cell memory. Nat Immunol 21, 1397–1407 (2020). [PubMed: 32989328]
26. Katagiri T, Kameda H, Nakano H & Yamazaki S Regulation of T cell differentiation by the AP-1 transcription factor JunB. Immunological Medicine 1–12 (2021) doi:10.1080/25785826.2021.1872838.
27. Zhao X, Shan Q & Xue H-H TCF1 in T cell immunity: a broadened frontier. Nat Rev Immunol (2021) doi:10.1038/s41577-021-00563-6.
28. Sudhamsu J et al. Dimerization of LT R by LT 1 2 is necessary and sufficient for signal transduction. Proceedings of the National Academy of Sciences 110, 19896–19901 (2013).
29. Li C et al. Structurally Distinct Recognition Motifs in Lymphotoxin-β Receptor and CD40 for Tumor Necrosis Factor Receptor-associated Factor (TRAF)-mediated Signaling. Journal of Biological Chemistry 278, 50523–50529 (2003). [PubMed: 14517219]

30. Wu M-Y, Wang P-Y, Han S-H & Hsieh S-L The Cytoplasmic Domain of the Lymphotoxin-β Receptor Mediates Cell Death in HeLa Cells. Journal of Biological Chemistry 274, 11868–11873 (1999). [PubMed: 10207006]
31. Macian F NFAT proteins: key regulators of T-cell development and function. Nat Rev Immunol 5, 472–484 (2005). [PubMed: 15928679]
32. Dejardin E et al. The Lymphotoxin-β Receptor Induces Different Patterns of Gene Expression via Two NF-κB Pathways. Immunity 17, 525–535 (2002). [PubMed: 12387745]
33. Saoulli K et al. CD28-independent, TRAF2-dependent Costimulation of Resting T Cells by 4-1BB Ligand. Journal of Experimental Medicine 187, 1849–1862 (1998). [PubMed: 9607925]
34. Thommen DS & Schumacher TN T Cell Dysfunction in Cancer. Cancer Cell 33, 547–562 (2018). [PubMed: 29634943]
35. Roth TL et al. Pooled Knockin Targeting for Genome Engineering of Cellular Immunotherapies. Cell 181, 728–744.e21 (2020). [PubMed: 32302591]
36. VanArsdale TL et al. Lymphotoxin-receptor signaling complex: Role of tumor necrosis factor receptor-associated factor 3 recruitment in cell death and activation of nuclear factor B. Proceedings of the National Academy of Sciences 94, 2460–2465 (1997).
37. Yilmaz ZB et al. Quantitative Dissection and Modeling of the NF-κB p100-p105 Module Reveals Interdependent Precursor Proteolysis. Cell Reports 9, 1756–1769 (2014). [PubMed: 25482563]
38. Hu B et al. Augmentation of Antitumor Immunity by Human and Mouse CAR T Cells Secreting IL-18. Cell Reports 20, 3025–3033 (2017). [PubMed: 28954221]
39. Yeku OO, Purdon TJ, Koneru M, Spriggs D & Brentjens RJ Armored CAR T cells enhance antitumor efficacy and overcome the tumor microenvironment. Sci Rep 7, 10541 (2017). [PubMed: 28874817]
40. Lynn RC et al. c-Jun overexpression in CAR T cells induces exhaustion resistance. Nature 576, 293–300 (2019). [PubMed: 31802004]
41. Schmiedel BJ et al. Impact of Genetic Polymorphisms on Human Immune Cell Gene Expression. Cell 175, 1701–1715.e16 (2018). [PubMed: 30449622]

Additional References

42. Lissina A et al. Protein kinase inhibitors substantially improve the physical detection of T-cells with peptide-MHC tetramers. Journal of Immunological Methods 340, 11–24 (2009). [PubMed: 18929568]
43. Meier JA, Zhang F & Sanjana NE GUIDES: sgRNA design for loss-of-function screens. Nature Methods 14, 831–832 (2017). [PubMed: 28858339]
44. Liscovitch-Brauer N et al. Profiling the genetic determinants of chromatin accessibility with scalable single-cell CRISPR screens. Nat Biotechnol (2021) doi:10.1038/s41587-021-00902-x.
45. Dobin A et al. STAR: ultrafast universal RNA-seq aligner. Bioinformatics 29, 15–21 (2013). [PubMed: 23104886]
46. Legut M et al. High-Throughput Screens of PAM-Flexible Cas9 Variants for Gene Knockout and Transcriptional Modulation. Cell Reports 30, 2859–2868.e5 (2020). [PubMed: 32130891]
47. Langmead B, Trapnell C, Pop M & Salzberg SL Ultrafast and memory-efficient alignment of short DNA sequences to the human genome. Genome Biol 10, R25 (2009). [PubMed: 19261174]
48. Martin M Cutadapt removes adapter sequences from high-throughput sequencing reads. EMBnet j. 17, 10 (2011).
49. Wang B et al. Integrative analysis of pooled CRISPR genetic screens using MAGeCKFlute. Nat Protoc 14, 756–780 (2019). [PubMed: 30710114]
50. Love MI, Huber W & Anders S Moderated estimation of fold change and dispersion for RNA-seq data with DESeq2. Genome Biol 15, 550 (2014). [PubMed: 25516281]
51. Alexa A & Rahnenfuhrer. topGO: Enrichment Analysis for Gene Ontology. (2021).
52. Rambaldi D, Pece S & Di Fiore PP flowFit: a Bioconductor package to estimate proliferation in cell-tracking dye studies. Bioinformatics 30, 2060–2065 (2014). [PubMed: 24681909]

53. Wessels H-H et al. Massively parallel Cas13 screens reveal principles for guide RNA design. Nat Biotechnol 38, 722–727 (2020). [PubMed: 32518401]
54. Guedan S, Calderon H, Posey AD & Maus MV Engineering and Design of Chimeric Antigen Receptors. Molecular Therapy - Methods & Clinical Development 12, 145–156 (2019). [PubMed: 30666307]
55. Melsted P et al. Modular, efficient and constant-memory single-cell RNA-seq preprocessing. Nat Biotechnol (2021) doi: 10.1038/s41587-021-00870-2.
56. Melsted P, Ntranos V & Pachter L The barcode, UMI, set format and BUStools. Bioinformatics 35, 4472–4473 (2019). [PubMed: 31073610]
57. Langmead B & Salzberg SL Fast gapped-read alignment with Bowtie 2. Nat Methods 9, 357–359 (2012). [PubMed: 22388286]
58. Stoeckius M et al. Cell Hashing with barcoded antibodies enables multiplexing and doublet detection for single cell genomics. Genome Biol 19, 224 (2018). [PubMed: 30567574]
59. McGinnis CS et al. MULTI-seq: sample multiplexing for single-cell RNA sequencing using lipid-tagged indices. Nat Methods 16, 619–626 (2019). [PubMed: 31209384]
60. Hao Y et al. Integrated analysis of multimodal single-cell data. http://biorxiv.org/lookup/doi/10.1101/2020.10.12.335331 (2020) doi: 10.1101/2020.10.12.335331.
61. Chung NC & Storey JD Statistical significance of variables driving systematic variation in high-dimensional data. Bioinformatics 31, 545–554 (2015). [PubMed: 25336500]
62. Becht E et al. Dimensionality reduction for visualizing single-cell data using UMAP. Nat Biotechnol (2018) doi: 10.1038/nbt.4314.
63. Storey JD & Tibshirani R Statistical significance for genomewide studies. Proc Natl Acad Sci U S A 100, 9440–9445 (2003). [PubMed: 12883005]
64. Pallares LF, Picard S & Ayroles JF TM3'seq: A Tagmentation-Mediated 3' Sequencing Approach for Improving Scalability of RNAseq Experiments. G3 Genes|Genomes|Genetics 10, 143–150 (2020). [PubMed: 31676507]
65. Liscovitch-Brauer N et al. Profiling the genetic determinants of chromatin accessibility with scalable single-cell CRISPR screens. Nat Biotechnol 39, 1270–1277 (2021). [PubMed: 33927415]
66. Yates AD et al. Ensembl 2020. Nucleic Acids Research gkz966 (2019) doi:10.1093/nar/gkz966.
67. Soneson C, Love MI & Robinson MD Differential analyses for RNA-seq: transcript-level estimates improve gene-level inferences. F1000Res 4, 1521 (2015). [PubMed: 26925227]
68. Schneider VA et al. Evaluation of GRCh38 and de novo haploid genome assemblies demonstrates the enduring quality of the reference assembly. Genome Res. 27, 849–864 (2017). [PubMed: 28396521]
69. Li H et al. The Sequence Alignment/Map format and SAMtools. Bioinformatics 25, 2078–2079 (2009). [PubMed: 19505943]
70. Picard Toolkit. (GitHub Repository, 2019).
71. Zhang Y et al. Model-based Analysis of ChIP-Seq (MACS). Genome Biol 9, R137 (2008). [PubMed: 18798982]
72. Quinlan AR & Hall IM BEDTools: a flexible suite of utilities for comparing genomic features. Bioinformatics 26, 841–842 (2010). [PubMed: 20110278]
73. Schep AN, Wu B, Buenrostro JD & Greenleaf WJ chromVAR: inferring transcription-factor-associated accessibility from single-cell epigenomic data. Nat Methods 14, 975–978 (2017). [PubMed: 28825706]
74. Ramírez F, Dündar F, Diehl S, Grüning BA & Manke T deepTools: a flexible platform for exploring deep-sequencing data. Nucleic Acids Research 42, W187–W191 (2014). [PubMed: 24799436]
75. Lopez-Delisle L et al. pyGenomeTracks: reproducible plots for multivariate genomic datasets. Bioinformatics 37, 422–423 (2021). [PubMed: 32745185]

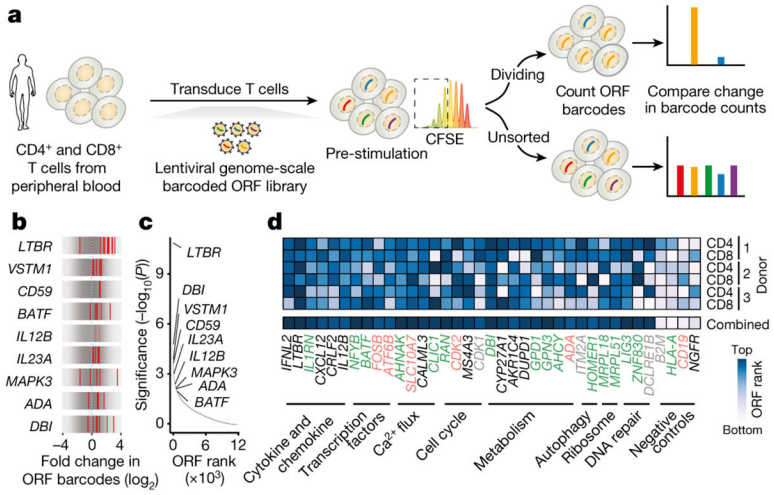

Figure 1. A genome-scale overexpression screen to identify genes that boost proliferation of primary human T-cells.

(**a**) Overview of the pooled open reading frame (ORF) screen. CD4+ and CD8+ T-cells were separately isolated from peripheral blood from three healthy donors. Barcoded genome-scale ORF library was then introduced into CD3/CD28-stimulated T-cells, followed by selection of transduced cells. After 14 days of culture, T-cells were labelled with carboxyfluorescein succinimidyl ester (CFSE) and re-stimulated to induce proliferation. By comparing counts of specific ORF barcodes before and after cell sorting, we identified ORFs enriched in the $CFSE^{low}$ population. (**b**) Normalised enrichment of individual barcodes for indicated genes in the CD4+ screen. (**c**) Robust rank aggregation of genes in both $CFSE^{low}$ CD4+ and CD8+ T-cells based on consistent enrichment of individual barcodes for each gene. (**d**) Enrichment in individual donors and T-cell populations of top-ranked genes (grouped by function and relevance to T-cell proliferation) selected for further study. Neutral genes (MHC-I complex and cell-type specific differentiation markers) are included for comparison. Gene names are coloured based on the differential expression in CD3/CD28-stimulated and resting T cells (*green*: up-regulated, *red*: down-regulated, *grey*: no change, *black:* no expression)[41].

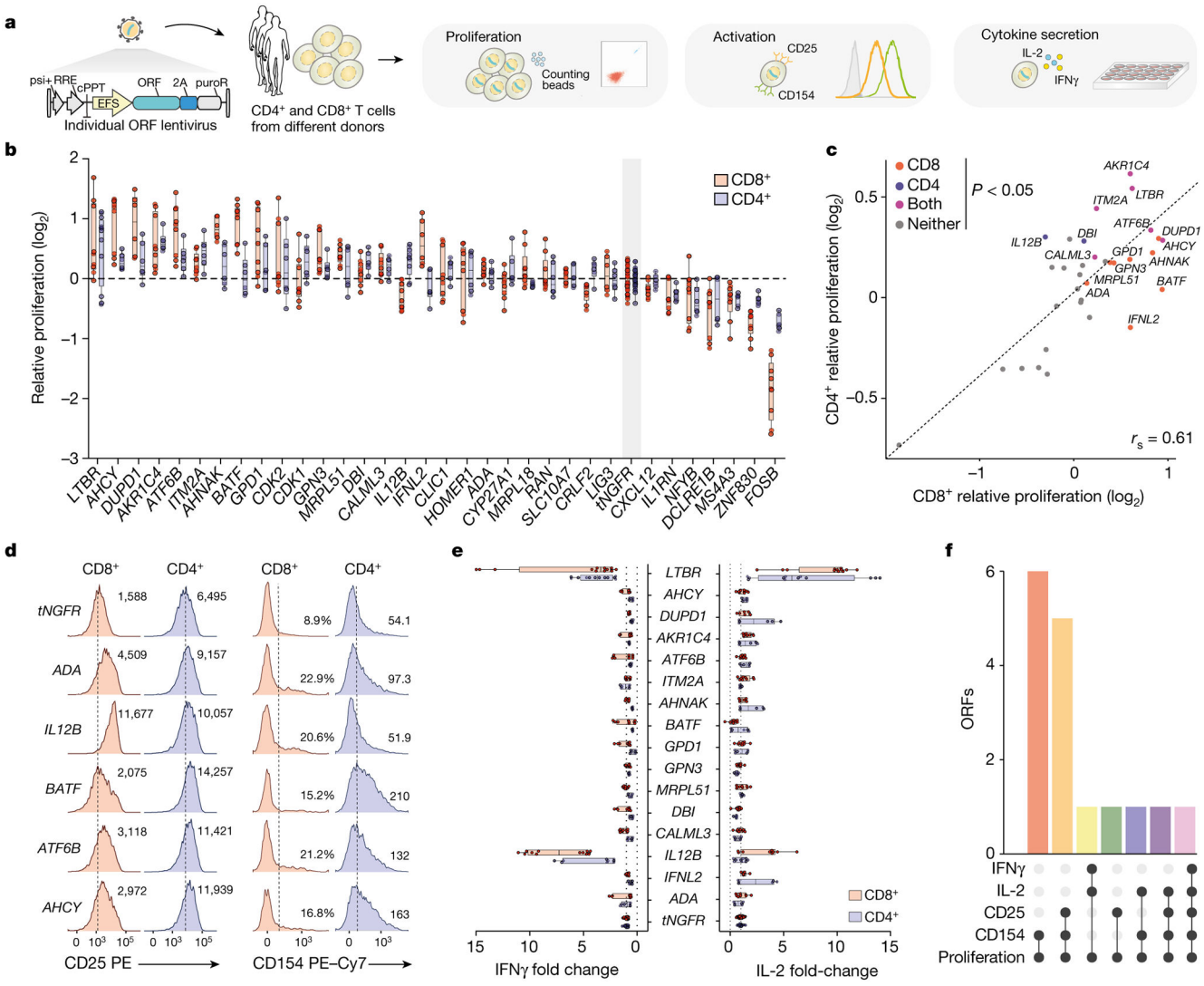

Figure 2. Overexpression of top-ranked ORFs increases proliferation, activation, and cytokine secretion of CD4+ and CD8+ T-cells.

(**a**) CD4+ and CD8+ T-cells from screen-independent donors were separately isolated and then transduced with lentiviruses encoding top-ranked ORFs together with a selection marker. Following transduction and selection, T-cells were re-stimulated before measurement of proliferation, expression of activation markers, and cytokine secretion. (**b**) Proliferation of T-cells transduced with top-ranked genes as fold change in absolute cell numbers of stimulated cells versus the corresponding unstimulated control, normalised to tNGFR. A minimum of two donors was tested per overexpressed gene, in biological triplicate. Box shows 25-75 percentile with a line at the mean while whiskers extend to maximum and minimum values. (**c**) Mean proliferation of ORF-transduced T-cells in CD4+ and CD8+ T-cells, normalised to tNGFR. Significant genes in both or either T-cell subsets are marked (Student's two-sided *t* test $p < 0.05$ and false discovery rate < 0.1). (**d**) Representative expression of CD25 or CD154 following re-stimulation. The numbers on histograms correspond to the percentage of gated cells (CD8+ CD154+) or the mean fluorescence intensity (MFI). Dashed lines indicate the gate used to enumerate CD154+ cells

(CD8+) or MFI for control (tNGFR) cells. (**e**) IL-2 and IFNγ secretion after re-stimulation, normalised to tNGFR. Only genes that significant increase T-cell proliferation in CD4+, CD8+ or both T-cell subsets are shown. A minimum of two donors was tested in triplicate per gene. Box shows 25-75 percentile with a line at the mean while whiskers extend to maximum and minimum values. (**f**) Intersection between different T-cell activation phenotypes significantly ($p < 0.05$) improved by a given ORF in CD8+ or CD4+ T-cells. Mean $\log_2$ fold change, two-sided *t* test *p* value and false-discovery rate for each ORF and phenotype are shown in Supplementary Table 6.

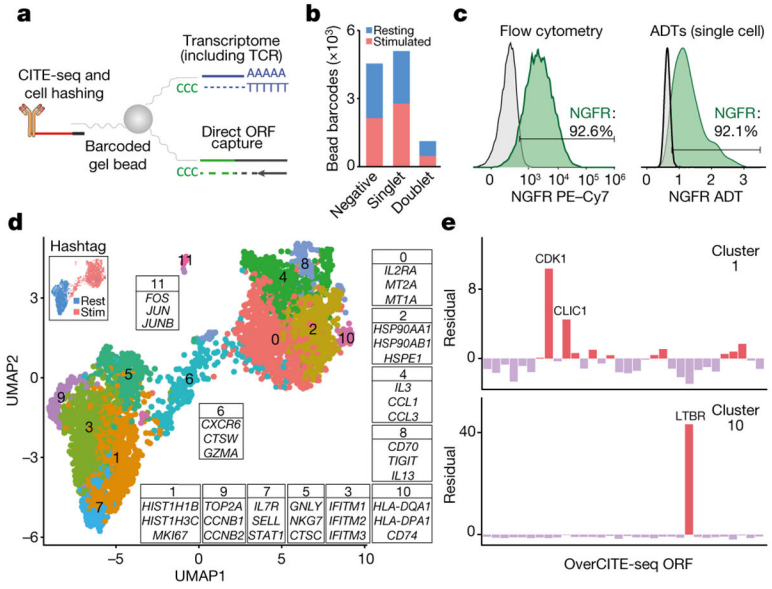

Figure 3. Single-cell OverCITE-seq identifies shared and distinct transcriptional programs induced by gene overexpression in T-cells.

(**a**) OverCITE-seq captures overexpression (ORF) constructs, transcriptomes, TCR clonotypes, cell-surface proteins, and treatment hashtags in single cells. (**b**) ORF assignment rate in resting and CD3/28-stimulated T-cells. (**c**) Antibody-tag sequencing (*right*) yields similar NGFR expression in tNGFR-transduced T-cells as flow cytometry (*left*) with tNGFR-transduced T-cells. Untransduced cells (*left*) or cells assigned a non-tNGFR ORF (*right*) are shown in grey. (**d**) UMAP representation of single cell transcriptomes after unsupervised clustering of OverCITE-seq captured ORF singlets. The inset in top left identifies stimulated and resting T-cells as given by treatment hashtags. For each cluster, a subset of the top 20 differentially expressed genes is shown. (**e**) ORF prevalence in two representative clusters. Standardised residual values are from a chi-squared test. ORFs of interest are shown.

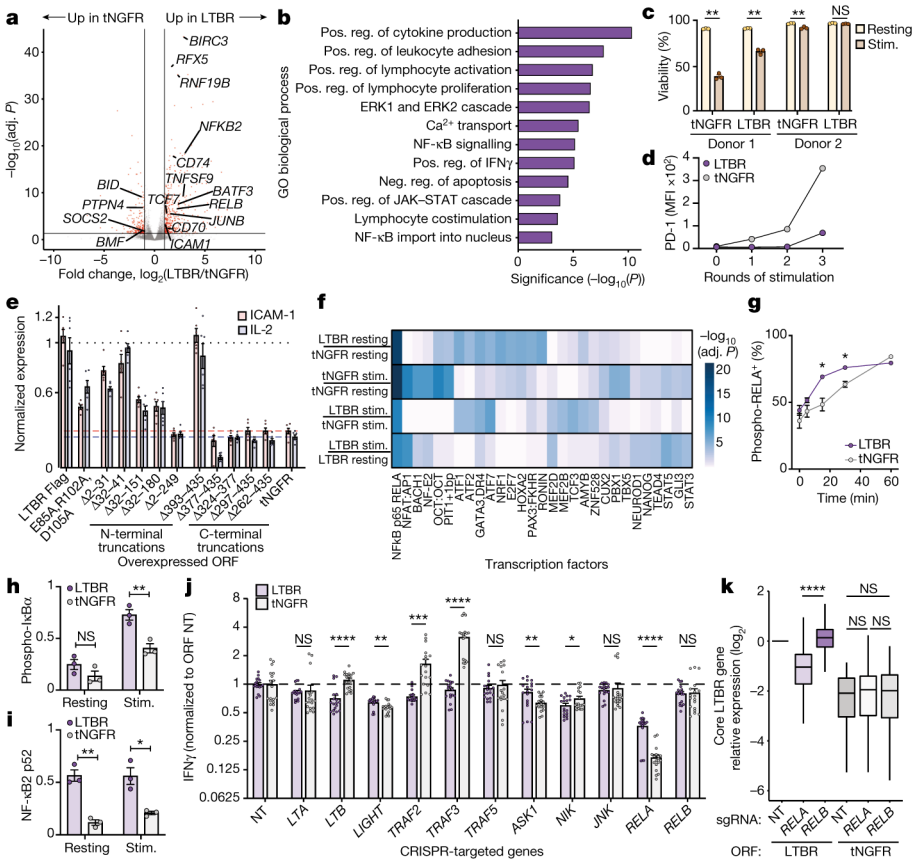

Figure 4. LTBR overexpression improves T-cell function via canonical NF-κB activation.

(**a**) Differential expression of genes in resting LTBR and tNGFR (negative control) T-cells. Genes highlighted in red are those with a 2-fold or greater change in expression and an adjusted $p < 0.05$. (**b**) Significantly enriched Gene Ontology biological processes in LTBR overexpressing T-cells ($p < 0.05$). (**c**) Cell viability of CD8+ T-cells transduced with LTBR or tNGFR lentivirus, either re-stimulated with CD3/CD28 for four days or left unstimulated ($n = 2$ donors with 3 biological replicates each). (**d**) PD-1 expression on resting LTBR or tNGFR T-cells stimulated with a 3:1 excess CD3/CD28 beads every 3 days, for up to 3 rounds of consecutive stimulation. (**e**) ICAM-1 expression (resting) and IL-2 secretion (activated) by T-cells transduced with FLAG-tagged LTBR mutants, normalised to wild-type LTBR ($n = 6$ replicates across two experiments). (**f**) Enrichment of transcription factor motifs in differentially accessible chromatin (top 10 motifs from each comparison). (**g**) Quantification of phospho-RelA in LTBR or tNGFR T-cells stimulated with CD3/CD28 antibodies for indicated periods of time. (**h**, **i**) Quantification of phosphorylated IκBα (*h*) or mature NF-κB2 (*i*) in resting or CD3/CD28-stimulated (15 minutes) LTBR or tNGFR cells. (**j**) IFNγ secretion by stimulated LTBR or tNGFR cells after CRISPR knockout of indicated genes ($n = 18$, 3 sgRNAs in 2 donors in 3 biological replicates). IFNγ quantities are normalised to corresponding non-targeting controls (either LTBR or tNGFR) to allow comparisons of relative impacts of gene knockout on T-cell activation. (**k**) Expression levels of core LTBR genes ($n = 274$ genes) in LTBR and tNGFR cells after CRISPR knockout of RELA or RELB (normalized to non-targeting controls). Box shows 25-75 percentile with a

line at the median while whiskers extend to 1.5x of interquartile range. Unpaired two-sided *t* test *p* values (panels *c, g-k*): ns $p>0.05$, * $p<0.05$, ** $p<0.01$, *** $p<0.001$, **** $p<0.0001$ (exact *p* values are given in Supplementary Table 15). Error bars are SEM. $N = 3$ biological replicates, unless stated otherwise.

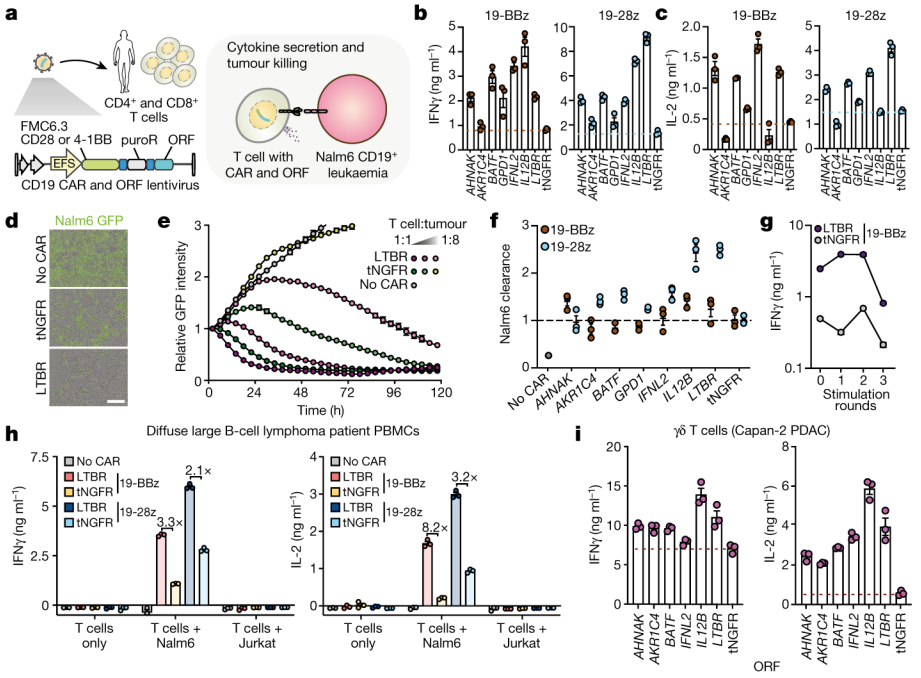

Figure 5. Top-ranked genes improve antigen-specific T-cell responses and tumour killing.

(**a** - **f**) Co-delivery of anti-CD19 CARs and ORFs to T-cells from healthy donors. (**b**) IFNγ and (**c**) IL2 secretion after overnight co-incubation of CD8+ T-cells with Nalm6 cells at 1:1 ratio (n = 3 biological replicates, representative of two donors). (**d**) Representative images of Nalm6 GFP+ cells co-incubated for 48 hours with CAR T-cells or untransduced control T-cells. Scale bar: 200 μm. (**e**) Nalm6 GFP+ cell proliferation (normalized total GFP per well) after co-incubation with T-cells co-expressing 19-28z CAR and LTBR or tNGFR (negative control) at the indicated effector to target ratios. (**f**) Quantification of Nalm6 GFP+ clearance for T-cells co-expressing 19-28z or 18-BBz CARs and top-ranked genes (n = 3 biological replicates, representative of two donors), normalised to tNGFR at effector to target ratio of 0.25 and after 48 hours of co-incubation. (**g**) 19-BBz CAR T-cells co-expressing LTBR or tNGFR were co-incubated at a 1:1 ratio with Nalm6 cells every three days for up to three rounds of stimulation (n = 3 biological replicates). Seven days after repeated antigen stimulation, CAR T-cells were re-exposed to Nalm6 cells. IFNγ secretion was measured after overnight incubation. **h**) Co-delivery of anti-CD19 CARs and ORFs to total PBMC from a diffuse large B-cell lymphoma patient. Transduced T-cells were incubated alone, or co-incubated with CD19+ Nalm6 or CD19− Jurkat cell lines at a 1:1 ratio (n = 3 biological replicates, representative of two patients). Secretion of IFNγ and IL2 was measured after overnight incubation and shown as fold increase of cytokine secretion by LTBR cells over tNGFR (negative control) cells. **i**) Delivery of ORFs to Vγ9Vδ2 T-cells. IFNγ and IL-2 secretion after overnight co-incubation with pancreatic ductal adenocarcinoma line Capan-2, pre-treated with zoledronate to boost phosphoantigen accumulation (n = 3 biological replicates).

Data are presented as mean values +/− SEM as appropriate.